(8) A. Streitwieser, U. Müller-Westerhoff, G. Sonnichsen, F. Mares, D. G. Morrell, K. O. Hodgson, and C. A. Harmon, *J. Am. Chem. Soc.*, **95**, 8644 (1973).
(9) A. Streitwieser, D. Dempf, G. N. La Mar, D. G. Karraker, and N. Edelstein, *J. Am. Chem. Soc.*, **93**, 7343 (1971).
(10) A. Streitwieser and C. A. Harmon, *Inorg. Chem.*, **12**, 1102 (1973).
(11) D. G. Karraker, *Inorg. Chem.*, **12**, 1105 (1973).
(12) A. Zalkin and K. N. Raymond, *J. Am. Chem. Soc.*, **91**, 5667 (1969); A. Avdeef, K. N. Raymond, K. O. Hodgson, and A. Zalkin, *Inorg. Chem.*, **11**, 1083 (1972).
(13) R. D. Fischer, *Theor. Chim. Acta*, **1**, 418 (1963).
(14) F. Mares, K. Hodgson, and A. Streitwieser, *J. Organomet. Chem.*, **24**, C68 (1970).
(15) K. O. Hodgson, F. Mares, D. F. Starks, and A. Streitwieser, *J. Am. Chem. Soc.*, **95**, 8650 (1973).
(16) K. O. Hodgson and K. N. Raymond, *Inorg. Chem.*, **11**, 3030 (1972).
(17) D. R. Scott and F. A. Matsen, *J. Phys. Chem.*, **72**, 16 (1968).
(18) K. D. Warren, *J. Phys. Chem.*, **77**, 1681 (1973).
(19) M. T. Hutchings and D. K. Ray, *Proc. Phys. Soc., London*, **81**, 663 (1963).
(20) R. J. Elliott and K. W. H. Stevens, *Proc. R. Soc. London, Ser. A*, **215**, 437 (1952).
(21) A. Abragam and B. Bleaney, "Electron Paramagnetic Resonance of Transition Ions", Oxford University Press, London, 1970.
(22) B. G. Wybourne, "Spectroscopic Properties of Rare Earths", Interscience, New York, N.Y., 1965.
(23) R. E. Watson and A. J. Freeman, *Phys. Rev.*, **127**, 2058 (1962).
(24) C. J. Lenander, *Phys. Rev.*, **130**, 1033 (1963).
(25) C. K. Jorgensen, "Orbitals in Atoms and Molecules", Academic Press, New York, N.Y., 1962.
(26) A. F. Orchard, *Faraday Discuss. Chem. Soc.*, **54**, 255 (1972); and private communication.
(27) L. Brewer, *J. Opt. Soc. Am.*, **61**, 1101, 1666 (1971); L. J. Radziemski, D. W. Steinhaus, R. D. Cowan, J. Blaise, G. Guelachvili, Z. B. Osman, and J. Verges, *ibid.*, **60**, 1556 (1970).
(28) Supplementary material.
(29) E. Clementi, "Tables of Atomic Functions", International Business Machines Corp., San Jose, Calif., 1965.
(30) D. W. Clack and W. Smith, *Rev. Roum. Chim.*, in press.
(31) F. A. Cotton, "Chemical Applications of Group Theory", Interscience, New York, N.Y., 1963.
(32) D. Brown, B. Whittaker, and N. Edelstein, *Inorg. Chem.*, **13**, 563, 1805 (1974).
(33) R. A. Satten, C. L. Schreiber, and E. Y. Wong, *J. Chem. Phys.*, **42**, 162 (1965).
(34) K. D. Warren, *Inorg. Chem.*, **13**, 1317 (1974).
(35) R. M. Golding, "Applied Wave Mechanics", Van Nostrand, New York, N.Y., 1969.
(36) D. G. Karraker and J. A. Stone, *J. Am. Chem. Soc.*, **96**, 6885 (1974).

Contribution from Bell Telephone Laboratories, Inc., Murray Hill, New Jersey 07974, and the Department of Chemistry, University of Wisconsin, Madison, Wisconsin 53706

Nonparameterized Molecular Orbital Calculations of Ligand-Bridged $Fe_2(CO)_6X_2$-Type Dimers Containing Metal–Metal Interactions[1,2]

BOON KENG TEO, MICHAEL B. HALL, RICHARD F. FENSKE, and LAWRENCE F. DAHL*

Received January 8, 1975 AIC50018C

Parameter-free molecular orbital calculations via the Fenske–Hall model have been carried out on representative Fe_2B_2-bridged complexes of the $Fe_2(CO)_6X_2$-type dimer (viz., those where X_2 denotes both the (B···B)-nonbonded $(SCH_3)_2$ and $(NH_2)_2$ ligands and the corresponding (B—B)-bonded S_2 and *cis*-$CH_3N{=}NCH_3$ ligands) and of the $[Fe_2(CO)_6(PR_2)_2]^n$ series (n = 0, 1−, 2−). These comparative calculations reveal that the above systematic variation of the bridging ligands (with and without direct B–B bonds) does not markedly affect the nature of the Fe–Fe interactions. The orbital character of the a_1 HOMO in each natural species is found to correspond closely to the classical "bent" Fe–Fe bond with the b_2 LUMO being its antibonding counterpart. Furthermore, the determined MO energy-level ordering and associated eigenvectors for the phosphido-bridged dimers with n = 1− and 2− are consistent with the monoanion possessing one electron and the dianion two electrons in this $4b_2$ MO of predominantly antibonding diiron character, corresponding formally to a "net" one-electron Fe–Fe bond and a "net" no-electron Fe–Fe bond, respectively. The results of this molecular orbital study, which provides the first detailed description of the electronic structure and bonding characteristics of this important dimeric metal cluster system, are evaluated and correlated with the available spectroscopic and crystallographic data.

Introduction

A large number of structurally related diiron hexacarbonyl complexes of general formula $Fe_2(CO)_6X_2$ containing Fe_2B_2-bridged systems (where B denotes the metal-attached bridging atom of ligand X) have been characterized by X-ray diffraction. These ligand-bridged diamagnetic species, which each possess an electron-pair Fe–Fe interaction, may be classified into the following two general groups: (a) dimers with no B–B bonds exemplified by either *two* separate, bridging X ligands, which are identical in the cases of NH_2,[3a] SR (with R = C_2H_5,[3b] C_6H_5[3c]), and PRR′ (with R = C_6H_5, R′ = CH_3 or H)[3d] and different as found for X = P(*p*-$CH_3C_6H_4$)$_2$, X′ = OH,[3e] or for one bidentate X_2 group such as $(NR)_2C{=}O$ (with R = CH_3,[3f] C_6H_5[3g]), $(NR)_2C{=}NR$ (with R = C_6H_{11}),[3h] RNC_6H_4NR' (with R = H, R′ = C_6H_5),[3i] $S_2C_2R_2$ (with R = C_6H_5),[3j] and $As_4(CH_3)_4$;[3k] (b) dimers with direct B–B bonds for which X_2 = $(NCH_3)_2$,[4a] $N_2C_{12}H_8$,[4b] $N_2C_5H_8$,[4c] and S_2.[4d] In all of these nitrogen-, sulfur-, phosphorus-, and arsenic-bridged dimers the local coordination about each iron atom may be described (with the neglect of Fe–Fe bonding) as a distorted tetragonal pyramid with two carbonyl ligands and the two bridging B atoms located in the basal plane and one axial carbonyl. The dimeric molecule, formally arising from the junction of the basal planes of the two tetragonal pyramids along the common B–B line, has a highly nonplanar Fe_2B_2 core with sharply acute Fe–B–Fe angles and a short Fe–Fe distance in the single-bond range. An important observed structural feature in these homologous complexes (Figure 1) is the general occurrence (in the absence of abnormal steric effects)[5] of a symmetrical Fe_2B_2-bridged fragment having idealized C_{2v} geometry with analogous Fe–Fe distances and resembling Fe–B–Fe angles for similar X ligands.

An electron-pair coupling interaction between the two Fe(I) atoms is necessary in order for each iron to attain a closed-shell electronic configuration in accord with the diamagnetic character of the compounds. In order to rationalize the basic geometry of these dimers, a *distinct* "bent" Fe–Fe bond was proposed[3a,b,4d] which was conceptually viewed as completing an octahedral-like coordination about each iron atom. Although this postulation of a *distinct* Fe–Fe bond in such complexes has gained general acceptance, its directional nature is still a subject of some controversy. From qualitative symmetry considerations Braterman[6] subsequently suggested that the nature of bonding in $Fe_2(CO)_6X_2$-type complexes is presumably closely related (on the basis of electronic bookkeeping) to that in the geometrically similar $Co_2(CO)_8$. Despite the absence of any simple conclusive argument, Braterman[6] felt drawn to the straight-bond model of $Co_2(CO)_8$

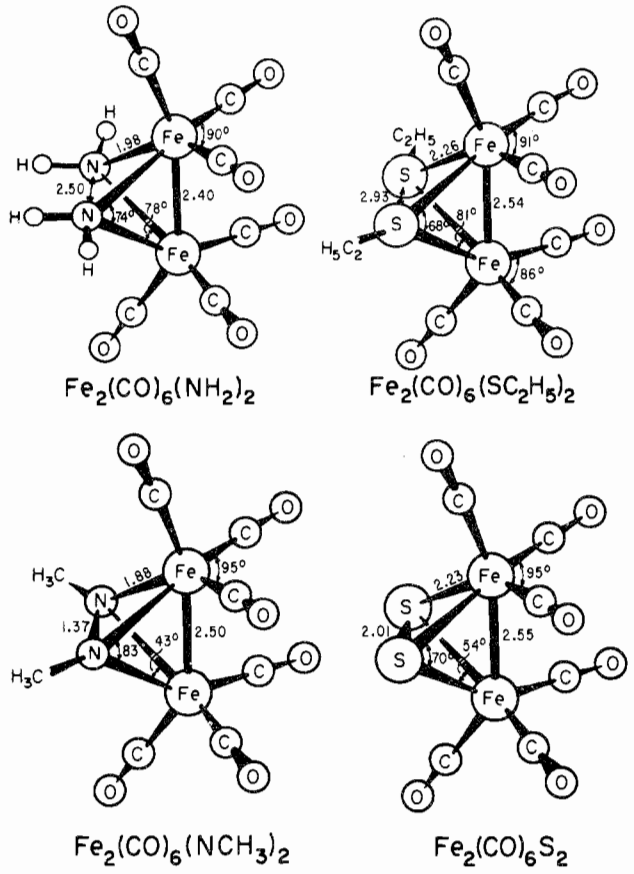

Figure 1. Molecular geometries of representative $Fe_2(CO)_6X_2$ molecules containing similarly deformed Fe_2B_2 cores both with and without direct B–B bonds.

because "of the analogy with these compounds where the presence of a straight bond has been established" (e.g., $Fe_2(CO)_9$ vs. $Co_2(CO)_8$) and "a dislike of assuming a nonbonded contact over a distance necessarily shorter than the total length of the bent bonds".

Although no distinction between a "straight" and a "bent" metal–metal bond model can be made for $Fe_2(CO)_6X_2$ complexes from symmetry considerations alone in that for both models the corresponding dimetal orbitals belong to the same irreducible representations under C_{2v} geometry, a differentiation between these models is possible from an examination of the electron density distributions in a number of these complexes. We present here the results of our theoretical investigation of representative complexes of the $Fe_2(CO)_6X_2$ series where X_2 denotes $(SCH_3)_2$, S_2, $(NH_2)_2$, and $(NCH_3)_2$ and of the $[Fe_2(CO)_6(PR_2)_2]^n$ series (n = 0, 1–, 2–). Our inclusion of the latter anions (n = 1–, 2–) in the MO calculations was prompted from the recent work by Dessy and coworkers,[7] who electrochemically generated and spectroscopically characterized the mono- and dianions of $Fe_2(CO)_6(P(CH_3)_2)_2$. Of special interest was that they initially concluded[7a] from their data that the additional electrons in these anions go into a MO comprised mainly of bridging ligand character rather than occupy a MO mainly comprised of antibonding dimetal orbital character which was previously advocated by us[8] from structural analyses of ligand-bridged dimers with and without metal–metal bonds. In this light it was particularly intriguing to account theoretically for the fact that for these $[Fe_2(CO)_6(P(CH_3)_2)_2]^n$ (n = 0, 1–, 2–) dimers the Mössbauer spectra,[7a] which showed only small negative isomer shifts (viz., stepwise changes of −0.06 and −0.19 mm/sec at −196°) with variation from n = 0 to 1– to 2–, indicated relatively little changes in iron charge upon reduction. Hence, our primary objectives in the work presented here included not only the hope of resolving the specific nature of the metal–metal bond in this type of complex but also an elucidation of the electronic interrelationships of these dimeric cluster systems upon systematic variation of the X ligands with and without B–B bonds and upon reduction.

Experimental Section

The Molecular Orbital Method. The particular computational program used was that developed by Fenske and Hall.[9] The method is an approximate Hartree–Fock–Roothaan SCF–LCAO molecular orbital approach which involves no arbitrary or adjustable parameters and is dependent only upon the choice of wave functions and atomic coordinates as input data. The operation is a self-consistent one, and the calculations were iterated until the absolute value of the difference in the Mulliken population in each valence orbital was less than 0.005. The computer program is not limited to any particular symmetry, and the results are rotationally invariant to the atomic coordinate systems employed.

Basis Functions. The utilized basis functions for the free atoms included the 3d, 4s, and 4p AO's as valence orbitals for iron with all inner AO's taken as "frozen" atomic core orbitals. Similarly, for each of the ligand atoms the outermost s and p AO's were employed as valence orbitals with the inner ones frozen to their atomic form. The carbon, nitrogen, and oxygen functions are those of Clementi,[10] where the 1s and 2s orbitals were curve fit to reduce the number of exponents from 2 to 1. The sulfur and phosphorus functions were also obtained by a curve fitting of Clementi's functions[10] to single-ζ form for the 1s to 3s functions and to double-ζ form for the 3p functions. The utilized exponent of 1.2 for the hydrogen 1s orbital corresponds to the minimum energy exponent for methane.[11] The 1s through 3d functions for iron were taken from the work of Richardson et al.[12] with the 3d function corresponding to a $3d^7$ configuration of Fe(I). The 4s and 4p iron functions were taken to have exponents of 2.1 and 1.7, respectively, corresponding to those utilized by Hall and Fenske[13] in their MO calculations of the iron pentacarbonyl halide cations. All of these functions, which in each case were Schmidt-orthogonalized (beginning with the 1s function), are similar with those utilized previously in MO calculations via the Fenske–Hall model on other transition metal complexes.[2,9,13,14]

Molecular Parameters. The interatomic distances and angles used for $Fe_2(CO)_6(NCH_3)_2$ (I),[4a] $Fe_2(CO)_6(NH_2)_2$ (II),[3a] and $Fe_2(CO)_6S_2$ (III)[4d] were based upon their structural determinations, while those for $Fe_2(CO)_6(SCH_3)_2$ (IV) and $Fe_2(CO)_6(PH_2)_2$ (V) were inferred from the structurally analogous species $Fe_2(CO)_6(SC_2H_5)_2$[3b] and $Fe_2(CO)_6[P(CH_3)(C_6H_5)]_2$,[3d] respectively. These replacements of the phenyl and methyl substituents with hydrogens in the phosphido-bridged dimer and of the anti ethyl substituents with methyls in the mercapto-bridged dimer were made in order to simplify the calculations. The MO calculations for these and other ligand-bridged dimers show that the energy levels and corresponding orbital characters (especially those primarily metallic in character) are relatively insensitive to whether R is C_6H_5, CH_3, or H. Related bond angles were averaged so that the atomic coordinates conformed to an idealized C_{2v} geometry (except for $Fe_2(CO)_6(SCH_3)_2$ which with inclusion of the anti CH_3 substituents has its symmetry lowered from C_{2v} to C_s-m). In order to facilitate a comparison among these species, the two $Fe(CO)_3$ moieties in each case were treated as "rigid" groups with fixed Fe–C and C–O bond lengths of 1.78 and 1.15 Å, respectively, and with fixed C(ax)–Fe–C(eq), C(eq)–Fe–C(eq), and C(ax)–Fe–X bond angles of 98.9, 92.2, and 103.2°, respectively. These values, obtained from an averaging of appropriate bond lengths and angles of known structures, are in accord with their small ranges of 1.77–1.81 Å, 1.14–1.17 Å, 97.5–100.2°, 88.7–95.3°, and 101.0–104.6°, respectively. The average Fe–Fe, Fe–B, and B···B distances of the Fe_2B_2 cores are listed in Table I.

The molecular parameters used for the mono- and dianion species (for which hydrogen substituents were again substituted in place of the methyl groups on the phosphorus atoms) require some comments. Since no analogous structural data are available at the present time for an $Fe_2(CO)_6X_2$ dimer to which one or two electrons have been added, the following assumptions were made upon reduction of the neutral $Fe_2(CO)_6(PH_2)_2$ molecule. (1) The iron–iron distance was assumed to increase stepwise from an electron-pair value of 2.62 Å to a half-bonding value of 2.99 Å to a nonbonding value of 3.36 Å.

Table I. Mean Geometrical Parameters Used for the MO Calculations

No.	Complex	Assumed symmetry	Ref structure	Fe-Fe, Å	Fe-B,[a] Å	B···B, Å	ρ,[b] deg	Ref
I	$Fe_2(CO)_6(NCH_3)_2$	C_{2v}	Same	2.496 (3)	1.878 (3)	1.366 (8)	31.3	4a
II	$Fe_2(CO)_6(NH_2)_2$	C_{2v}	Same	2.402 (6)	1.98 (1)	2.50 (3)	34.3	3a
III	$Fe_2(CO)_6S_2$	C_{2v}	Same	2.552 (2)	2.228 (4)	2.007 (5)	25.0	4d
IV	$Fe_2(CO)_6(SCH_3)_2$	Anti, C_s[c] Syn, C_{2v}	*anti*-$Fe_2(CO)_6(SC_2H_5)_2$	2.54 (1)	2.26 (1)	2.93 (1)	30.0	3b
V	$Fe_2(CO)_6(PH_2)_2$	C_{2v}	$Fe_2(CO)_6[P(CH_3)(C_6H_5)]_2$	2.619 (1)	2.218 (2)	2.864 (2)	33.2	3d
VI	$[Fe_2(CO)_6(PH_2)_2]^-$	C_{2v}		(2.99)[d]	(2.19)	(2.77)	(44.5)	
VII	$[Fe_2(CO)_6(PH_2)_2]^{2-}$	C_{2v}		(3.36)	(2.17)	(2.68)	(64.0)	

[a] B denotes the metal-attached atom of the bridging X ligand. [b] The angle between the Fe-Fe and Fe-CO(axial) vectors. [c] Symmetry imposed on the anti or biaxial syn isomer by inclusion of the two CH_3 substituents on the C_{2v} $Fe_2(CO)_6(S)_2$ fragment. [d] Values in parentheses were assumed from stereochemical considerations.

These latter values are typical of iron–iron distances found in related iron dimers with "net" one-electron and "net" no-electron iron–iron bonds.[15] (2) The P···P distance was assumed to decrease from 2.86 to 2.77 to 2.68 Å, in accord with the observed decrease of 0.18 Å in the nonbonding P···P distance in going from the phosphido-bridged $Co_2(\eta^5\text{-}C_5H_5)_2(P(C_6H_5)_2)_2$ (2.88 Å) to $Ni_2(\eta^5\text{-}C_5H_5)_2(P(C_6H_5)_2)_2$ (2.70 Å).[8] These latter two compounds are electronically equivalent to $[Fe_2(CO)_6(PH_2)_2]^n$ where n = 0 and 2−, respectively. (3) The Fe–P distances were assumed to decrease slightly from 2.22 to 2.19 to 2.17 Å, respectively, in accord with the general trend (observed[3j] first in the Fe_2S_2 dimers and later shown[4a-c] conclusively in the Fe_2N_2 dimers) that longer Fe–Fe bonds give rise to shorter Fe–B bonds. With these assumptions, the calculated P–M–P angles decrease slightly from 80.4 to 77.5°, while the dihedral angle formed by the two FeB_2 planes increases from 101.3 to 120.4 to 161.8°. The maintenance of the nonplanarity of the Fe_2B_2 fragment in the charged species is also in accord with the spectroscopic findings[7] that the exo and endo positions are not equivalent in the two anionic species (n = 1−, 2−) of $Fe_2(CO)_6(P(CH_3)_2)_2$.

Other structural parameters related to the bridging ligand(s) were either obtained from the known structures or reasonably assumed as follows. For $Fe_2(CO)_6(NCH_3)_2$[4a] the structural findings of an N–C bond length of 1.476 Å and an N–N–C bond angle of 123.0° were used along with idealized C–H distances of 1.08 Å and idealized H–C–H and N–C–H angles of 109.5°. For $Fe_2(CO)_6(SCH_3)_2$, an S–C bond length of 1.81 Å and Fe–S–C bond angles of 113.5° were taken from the structural determination of the ethyl analogue together with assumed values of 1.08 Å for the C–H distances and 109.5° for both the S–C–H and H–C–H bond angles. For $Fe_2(CO)_6(NH_2)_2$ and $[Fe_2(CO)_6(PH_2)_2]^n$, N–H and P–H bond lengths of 1.01 and 1.44 Å[16] were used, while the H–N–H and H–P–H angles were fixed at 107.0 and 101.5°, respectively.

The local Cartesian coordinate systems for each dimer were chosen as follows: (1) the z axis of each iron atom was oriented along the Fe–CO(axial) line but in the opposite direction, while the y axis lies in the plane passing through the two iron atoms and the midpoint of the two bridging atoms; (2) the z axis of each bridging B atom was pointed toward the midpoint of the two iron atoms, and the y axis was directed parallel to the Fe–Fe vector; (3) the z axis of each carbonyl carbon and oxygen atom was directed toward the iron atom, and the y axis was chosen to lie in the plane containing the two iron atoms and the atom under consideration; (4) the z axis of an atom attached to a bridging atom was directed toward the bridging atom, and the y axis was directed parallel to the Fe–Fe vector; (5) the x axes of all atoms were determined by the right-handed rule.

Results and Discussion

Free Carbonyl and Bridging Ligands. After completion of each calculation in the atomic set, the final canonical molecular orbitals were transformed into a basis set involving the molecular orbitals of the isolated carbonyl and bridging ligands. This free-ligand representation, which facilitates a direct comparison of the polyatomic ligands before and after metal complexation, has been widely utilized in successful correlations of bonding trends in other transition metal complexes.[2,9,13,14] The procedure effectively isolates the population changes in those few ligand orbitals which are primarily involved in bonding to the metal and/or other atoms in the complex such that only the free-ligand molecular orbitals which are close in energy and which overlap significantly with the metal orbitals will be affected appreciably. The molecular orbitals for the free carbonyl and free bridging polyatomic ligands were calculated on the basis of each ligand being depicted as a neutral entity with the same geometry and molecular parameters as utilized for the ligand in each metal complex. Since calculations made with each bridging ligand treated either as a neutral radical or as an anion showed no serious differences in the orbital character of the free ligand, our choice of the transformational basis was made on the premise that the orbital populations[17] and atomic charges[17] in the metal dimers are closer to those in the neutral free bridging ligands. Table II lists the percent characters, eigenvalues, and overlap populations for those particular free-ligand orbitals found by our calculations to be involved in the metal–ligand bonding together with the Mulliken gross atomic charges.

Previous MO calculations have shown that only three carbon monoxide MO's possess the appropriate symmetry and energy to interact strongly with the metal orbitals—viz., the highest occupied MO (HOMO) of representation 5σ, which forms a σ bond by electron-pair donation to the unfilled metal orbitals, and the two doubly degenerate, lowest unoccupied MO's (LUMO's) of 2π (or π^*) representation, which form partial π bonds by back-bonding from the filled metal d orbitals.[9,13,14a-f] The fact that the overlap populations reveal that the 5σ and 2π MO's of carbon monoxide are both antibonding in character implies[9] that electron donation from the 5σ orbital to the metal will strengthen the C–O bond whereas back-donation of electron density from the metal to the 2π orbitals will weaken the C–O bond. Prior molecular orbital studies via the Fenske–Hall model not only have substantiated these conclusions concerning the opposing effects of the σ- and π-bonding process on the C–O bond strength in a metal carbonyl complex but also have demonstrated for a series of metal carbonyl halide and dihalide complexes that trends in the force constants of the carbonyl ligands could be accounted for only when changes in both the 5σ and 2π orbital occupations were considered.[9,13,14a-f] The determined correlation between the carbonyl force constants and orbital occupations in the $Fe_2(CO)_6X_2$ complexes is given later in this paper.

The Neutral $Fe_2(CO)_6X_2$ Complexes. (a) Nature of the Metal–Metal Bond. On the basis of a detailed stereochemical analysis, Dahl and coworkers[3a,b,4d] postulated that a *distinct* electron-pair metal–metal bond must be responsible for the molecular geometry of the $Fe_2(CO)_6X_2$ type of complex (with or without a direct B–B bond). For the $Fe_2(CO)_6(SC_2H_5)_2$ and $Fe_2(CO)_6(NH_2)_2$ molecules without B–B bonds, they also proposed a "bent" Fe–Fe bond conceptually involving the overlap of octahedral-like orbitals. The extent of the bending of the Fe–Fe bond was estimated from the assumption that the participating metal orbital for each iron is collinear with the trans axial carbonyl ligand. For $Fe_2(CO)_6S_2$ which exemplifies a dimer with a B–B bond, they pointed out that two

Table II. Percent Character, Eigenvalues, and Overlap Populations of the Pertinent Molecular Orbitals and Mulliken Gross Atomic Charges for the Free Ligands

Ligand	Symmetry	Orbital	Percent orbital character	Eigenvalue	Overlap population[a] between B···B	Mulliken gross atomic charges
CO	$C_{\infty v}$	5σ	s(C), 34.5; p_z(C), 47.7; s(O), 1.0; p_z(C), 16.9	−13.87	−0.121	$C^{0.08-}O^{0.08+}$
		2π	p(C), 67.2; p(O), 32.8	−0.53	−0.454	
cis-$CH_3N{=}NCH_3$	C_{2v}	$2b_2$	p_y(N), 2 × 45.9;[b] s(H), 4 × 1.8	−14.87	0.180	$N^{0.09-}C^{0.06+}$
		$5a_1$	s(N), 2 × 2.3; p_x(N), 2 × 36.8; p_z(N), 2 × 7.3; s(H), 2 × 2.1; 4 × 0.6	−14.46	0.108	$H^{0.01+}$
		$4b_1$	s(N), 2 × 5.6; p_x(N), 2 × 20.3; p_z(N), 2 × 17.8; p_z(C), 2 × 4.6	−9.68	−0.059	
		$2a_2$	p_y(N), 2 × 47.5; s(H), 4 × 1.3	−4.59	−0.284	
NH_2	C_{2v}	$2a_1$	s(N), 11.5; p_z(N), 82.2; s(H), 2 × 3.1	−14.87		$N^{0.25-}H^{0.12+}$
		$1b_2$	p_y(N), 100	−12.25		
S_2	$D_{\infty h}$	$1\pi_u$	p(S), 2 × 50	−14.27	0.167	S^0
		$2\sigma_g$	s(S), 2 × 6.5; p_z(S), 2 × 43.5	−13.72	0.007	
		$1\pi_g$	p(S), 2 × 50	−7.54	−0.252	
SCH_3	C_{3v}[c]	$3a_1$	s(S), 14.3; p_z(S), 61.1; p_z(C), 21.5; s(H), 3 × 0.7	−15.45		$S^{0.05-}C^{0.01-}H^{0.02+}$
		2e	$p_{x,y}$(S), 96.7; s(H), 2 × 1.6	−10.64		
PH_2	C_{2v}	$2a_1$	s(P), 19.5; p_z(P), 70.5; s(H) 2 × 5.0	−12.55		$P^{0.06+}H^{0.03-}$
		$1b_2$	p_y(P), 100	−9.44		
		$2b_1$	p_x(P), 54.8; s(H), 2 × 22.6	21.29		
		$3a_1$	s(P), 21.6; p_z(P), 26.8; s(H), 2 × 25.8	32.27		

[a] The overlap populations correspond to a single electron occupying the molecular orbital under consideration. [b] *n* times a value implies that there are *n* symmetry-related atomic orbitals with the same percent character. [c] In the MO calculation of free SCH_3 the *z* axes of both the S and C atoms are oriented along the threefold axis.

formal representations of the bonding arrangement about each iron atom can be invoked in conjunction with an analogously bent Fe–Fe bond. In one description each iron was again assumed to possess octahedral-like valency with two equivalent iron orbitals directed toward the bridging S_2 group. In the other model a σ–π formulation similar to the one first employed by Brown[18] to describe the dimetal–acetylene interaction in $Co_2(CO)_6(C_6H_5C_2C_6H_5)$ was suggested in which each iron atom is viewed as possessing a trigonal-bipyramidal valency with one equatorial hybrid orbital directed toward the center of the B–B bond. Although Wei and Dahl[4d] emphasized that these two limiting representations are only approximations, they suggested in the case of $Fe_2(CO)_6S_2$ that the actual electron density distribution about each iron atom in $Fe_2(CO)_6S_2$ may not differ appreciably from that in $Fe_2(CO)_6(SC_2H_5)_2$ in that the average value of 94.6° for the two equatorial OC–Fe–CO bond angles in $Fe_2(CO)_6S_2$, which is somewhat larger than the corresponding value of 88.7° in $Fe_2(CO)_6(SC_2H_5)_2$, is much nearer the idealized value of 90° expected for octahedral metal valency rather than the idealized value of 120° based on trigonal-bipyramidal metal valency.

On the other hand, a simple straight Fe–Fe bond description was subsequently suggested by Braterman[6] for the $Fe_2(CO)_6(SR)_2$, $Fe_2(CO)_6S_2$, and $Fe_2(CO)_6(PR_2)_2$ molecules on account of these dimers being similar in geometry to $Co_2(CO)_8$, for which, from the electronic bookkeeping, Braterman[6] presumed the nature of bonding to be closely related.[19,20] The straight metal–metal bond picture was preferred by Braterman[6] for $Co_2(CO)_8$ partly because it treats $Co_2(CO)_8$ as more closely analogous to $Fe_2(CO)_9$.

Despite expected differences arising between the Fe_2B_2 dimers with no B–B bonds and those with B–B bonds, the molecular orbital correlation diagrams (portrayed in Figure 2) for $Fe_2(CO)_6(NH_2)_2$ and the syn and anti isomers of $Fe_2(CO)_6(SCH_3)_2$ are surprisingly similar in their energy-level patterns to those for $Fe_2(CO)_6(NCH_3)_2$ and $Fe_2(CO)_6S_2$. In particular, the upper filled MO's can be divided into three sets of levels. The first set consists of seven completely filled MO levels with mainly iron 3d orbital character followed by a second lower energy set of two MO levels which contain large bridging ligand character, the highly variable splitting between them being particularly sensitive to the nature of the bridging ligand. Below these levels lies a third set of levels which are comprised of MO's with primarily bridging ligand or 5σ carbonyl character. About 5 eV above the HOMO, there exists one virtual orbital (i.e., the LUMO) which (as will be seen from later discussions) plays a very important role in the stereochemical properties of the reduced iron dimers.

Examination of the percent character of the HOMO and the LUMO (Table III) reveals that they correspond closely to the bonding and antibonding counterparts of the bent metal–metal bond. The six closely spaced MO levels below the HOMO can be viewed as arising from the bonding and antibonding combinations of the six iron lone electron pairs (i.e., three on each iron atom); these orbitals are stabilized by ca. 1 eV with respect to the diagonal 3d iron term primarily as a result of back-bonding of charge into the antibonding 2π carbonyl orbitals. In contrast, the HOMO of mostly iron orbital character does contain a small quantity of antibonding Fe–CO(axial) σ-like orbital character (Table III), which destabilizes the HOMO with respect to the diagonal 3d iron term by ca. 0.5 eV. The splitting of ca. 5 eV between the HOMO and LUMO arises almost exclusively from the interaction between the "hybrid" metal orbitals (one on each iron atom), which are mainly composed of 20% d_{z^2} and 10% p_z AO's of each iron atom and which lie approximately along the extrapolation of the Fe–CO(axial) bond.[21,22] However, there is a distinction between the calculated results and the qualitative description of the classical bent Fe–Fe bond in a $Fe_2(CO)_6X_2$ molecule. While the Fe–Fe bond was arbitrarily assumed to arise from the overlap of the iron orbitals whose directions were extrapolated from the two Fe–CO(axial) bonds, an examination of the compositions of the HOMO and LUMO (compiled in Table III) indicates that these MO's also contain

Table III. Energy, Symmetry, and Percent Orbital Character of the HOMO and LUMO in Selected $Fe_2(CO)_6X_2$ Complexes

Complex	Energy, eV	Orbital	$3d_{z^2}$ (2)[a]	$3d_{yz}$ (2)	$3d_{x^2-y^2}$ (2)	4s (2)	$4p_y$ (2)	$4p_z$ (2)	Bridging ligand[b]	Axial CO (2)	Equatorial CO (4)
$Fe_2(CO)_6(NCH_3)_2$	−8.15	$5a_1$	21.7	2.6	2.0	0.4	0.3	13.0	$5a_1$ (0.4)	5σ (1.3)	$2\pi_y$ (3.4)
			(13.6)[d]	(12.0)	(0.7)	(0.4)	(5.6)	(7.7)		$2\pi_y$ (0.5)	$2\pi_x$ (0.1)
	−2.94	$5b_2$	19.5	6.8	0.4	0.4	0.1	6.3	$2b_2$ (3.3)	5σ (1.4)	$2\pi_y$ (4.9)
			(20.0)	(6.2)	(0.5)	(0.4)	(2.7)	(3.7)		$2\pi_y$ (2.2)	$2\pi_x$ (0.6)
$Fe_2(CO)_6(NH_2)_2$	−8.56	$5a_1$	22.1	1.0	1.1	0.5	0.2	13.9	$2a_1$ (0.0)	5σ (1.4)	$2\pi_y$ (3.9)
			(8.9)	(15.3)	(0.0)	(0.5)	(6.1)	(8.0)		$2\pi_y$ (0.1)	$2\pi_x$ (0.5)
	−2.96	$4b_2$	18.9	5.0	0.0	0.0	0.7	4.6	$1b_2$ (2 × 5.2)[b]	5σ (1.2)	$2\pi_y$ (2.8)
			(16.5)	(7.5)	(0.0)	(0.0)	(3.6)	(1.7)		$2\pi_y$ (3.7)	$2\pi_x$ (2.4)
$Fe_2(CO)_6S_2$	−8.20	$5a_1$	22.1	4.5	1.1	0.3	0.7	12.2	$1\pi_u$ (0.5)	5σ (1.1)	$2\pi_y$ (2.6)
			(22.0)	(4.7)	(1.2)	(0.3)	(4.9)	(7.9)		$2\pi_y$ (1.0)	$2\pi_x$ (0.2)
	−3.07	$4b_2$	21.4	6.3	0.3	0.1	0.3	6.3	$1\pi_u$ (4.3)	5σ (1.6)	$2\pi_y$ (4.0)
			(24.6)	(2.8)	(0.6)	(0.1)	(2.6)	(4.1)		$2\pi_y$ (1.5)	$2\pi_x$ (0.7)
anti-$Fe_2(CO)_6(SCH_3)_2$	−7.53	8a′	16.7	3.7	6.2	0.3	0.7	9.2	2e (1.1, 5.4)[c]	5σ (0.9)	$2\pi_y$ (2.6, 1.9)
			(12.1)	(10.0)	(4.3)	(0.3)	(5.0)	(4.9)	$3a_1$ (0.6, 1.5)	$2\pi_y$ (0.8)	
	−3.16	6a″	19.6	7.3	0.1	0.1	0.3	5.8	2e (4.2, 4.4)	5σ (1.4)	$2\pi_y$ (3.4)
			(23.6)	(3.3)	(0.0)	(0.1)	(2.8)	(3.2)		$2\pi_y$ (1.7)	$2\pi_x$ (1.3, 1.0)
syn-$Fe_2(CO)_6(SCH_3)_2$	−7.24	$5a_1$	16.9	4.9	6.0	0.2	1.2	8.5	2e (2 × 4.2)	5σ (1.0)	$2\pi_y$ (1.7)
			(13.7)	(9.3)	(4.9)	(0.2)	(5.7)	(3.9)		$2\pi_y$ (1.4)	
	−3.15	$4b_2$	19.5	7.4	0.1	0.1	0.3	5.8	2e (2 × 4.3)	5σ (1.4)	$2\pi_y$ (3.4)
			(23.6)	(3.4)	(0.0)	(0.1)	(2.8)	(3.2)		$2\pi_y$ (1.6)	$2\pi_x$ (1.3)
$Fe_2(CO)_6(PH_2)_2$	−7.74	$5a_1$	24.6	2.1	0.2	0.3	0.4	12.4	$2b_1$ (2 × 0.9)	5σ (0.7)	$2\pi_y$ (3.0)
			(14.2)	(12.6)	(0.1)	(0.3)	(6.2)	(6.6)		$2\pi_y$ (0.5)	$2\pi_x$ (0.7)
	−3.83	$4b_2$	17.3	11.0	1.0	0.8	0.0	6.9	$1b_2$ (2 × 2.6)	5σ (1.2)	$2\pi_y$ (3.8)
			(26.8)	(2.3)	(0.2)	(0.8)	(2.0)	(4.9)		$2\pi_y$ (0.6)	$2\pi_x$ (0.6)
$[Fe_2(CO)_6(PH_2)_2]^-$ [e]	−6.38	$5a_1$	24.5	3.7	0.2	0.1	0.7	10.1	$2b_1$ (2 × 1.8)	5σ (0.5)	$2\pi_y$ (2.1)
			(7.8)	(20.0)	(0.7)	(0.1)	(8.0)	(2.8)		$2\pi_y$ (1.3)	$2\pi_x$ (1.3)
	−5.80	$4b_2$	18.4	12.1	1.2	1.6	0.0	9.3	$1b_2$ (2 × 0.4)	5σ (0.6)	$2\pi_y$ (1.9)
			(21.1)	(9.7)	(0.8)	(1.6)	(4.2)	(5.0)		$2\pi_y$ (1.0)	$2\pi_x$ (0.9)
$[Fe_2(CO)_6(PH_2)_2]^{2-}$ [e]	−5.83	$5a_1$	23.6	5.1	0.4	0.2	0.6	8.7	$2b_1$ (2 × 3.7)	5σ (0.3)	$2\pi_y$ (1.0)
			(0.0)	(24.4)	(4.7)	(0.2)	(9.0)	(0.3)		$2\pi_y$ (1.8)	$2\pi_x$ (1.9)
	−5.79	$4b_2$	22.3	9.6	0.0	0.9	0.1	9.5	$1b_2$ (2 × 0.1)	5σ (0.3)	$2\pi_y$ (1.0)
			(1.5)	(25.8)	(4.6)	(0.9)	(8.7)	(1.0)		$2\pi_y$ (1.9)	$2\pi_x$ (1.7)

[a] The number n in parentheses means that there are n symmetry-related orbitals of the same percent character. [b] n times a value in parentheses means that there are n symmetry related orbitals of the same percent character. [c] For *anti*-$Fe_2(CO)_6(SCH_3)_2$, percents character of two bridging ligand orbitals are drastically different (due to breakdown of C_{2v} symmetry); hence they are listed separately. [d] The number in parentheses is the corresponding value when a standard diatomic coordinate system is used instead of the coordinate system specified in the text. [e] The orbital energies of the mono- and dianions of $Fe_2(CO)_6(PH_2)_2$ have been shifted by −4.75 and −9.50 eV, respectively such that the nonbonding CO 3σ levels are as those in the neutral molecule.

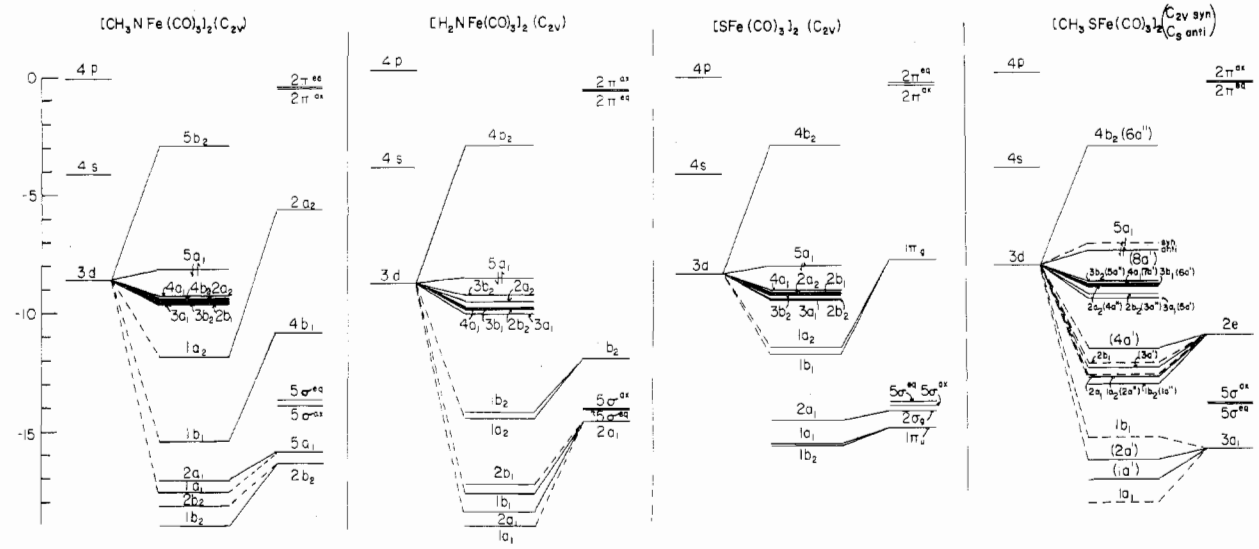

Figure 2. Molecular orbital energy level diagrams for $Fe_2(CO)_6(NH_2)_2$ and $Fe_2(CO)_6(SCH_3)_2$, which both contain separate bridging X ligands, and for $Fe_2(CO)_6(NCH_3)_2$ and $Fe_2(CO)_6S_2$, which both possess direct B–B bonds. The energy diagram for $Fe_2(CO)_6(SCH_3)_2$ shows the small energy changes manifested by whether the two methyl substituents possess an equatorial–axial anti configuration (corresponding to a C_s-*m* geometry) or a biaxial syn configuration (corresponding to a C_{2v}-2*mm* geometry) with two axially oriented S–CH_3 bonds. The irreducible representations for the syn isomer are given without parentheses and the corresponding ones for the anti isomer within parentheses.

Table IV. Comparison of the Bending Angle (θ) Obtained from the HOMO with the angle (ρ) between the Fe–Fe and Fe–CO(axial) Vectors

$Fe_2(CO)_6X_2$	ρ_{obsd},[a] deg	ρ,[b] deg	θ,[c] deg
$Fe_2(CO)_6(NCH_3)_2$	29.8	31.3	21.5
$Fe_2(CO)_6(NH_2)_2$	34.0	34.3	24.0
$Fe_2(CO)_6S_2$	25.0	25.0	15.2
anti-$Fe_2(CO)_6(SCH_3)_2$	33.5	30.0	19.0

[a] Value observed in structural determination. [b] The corresponding value based on the idealized geometry used in the present study. [c] The value measured from an electron density plot of the highest occupied molecular orbital.

significant d_{yz} AO's which add some "straight" Fe–Fe bonding character. When the localized coordinate systems on the two iron atoms are transformed into a standard diatomic coordinate system (such that the two z' axes point toward each other with the corresponding x' axes parallel), it is seen from Table III that the d_{z^2} orbitals decompose into a combination of $d_{z'^2}$ and $d_{y'z'}$, whereas the p_z orbitals transform into $p_{y'}$ and $p_{z'}$. Therefore, the larger percent character of d_{yz} in the original coordinates (or equivalently the larger percent character of $d_{z'^2}$ in the standard diatomic coordinates) implies a smaller degree of bending of the Fe–Fe bond. The degree of bending can also be assessed from a consideration of the angle θ made by the tangent (at each iron site) of the contour of maximum electron density[23] of the HOMO and the line joining the two iron atoms, as depicted in Figure 3 for $Fe_2(CO)_6S_2$. A comparison in Table IV of the bending angle θ for each dimer with the calculated angle ρ between the Fe–Fe and Fe–CO(axial) vectors shows in general that the Fe–Fe bond is not as "bent" as that assumed from an extrapolation of the Fe–CO(axial) bonds; rather, the bending angle (θ) is consistently smaller than ρ by ca. 10°. This angular relationship between θ and ρ is not unexpected, by reason of the Fe–CO bonds being much stronger than the Fe–Fe bond and thereby dictating the direction of the metal orbitals used for the metal–metal bonding. The variation of the bending angles θ from 19 to 24° for these iron dimers is not unreasonable in light of other similarly determined bent bonds such as that of 20° from the electron density plot of the two HOMO's (3e') in cyclopropane[24a] and 31 and 33° from the localized MO of bicyclobutane.[24b]

These calculations also agree with the conclusions reached from the crystallographic parameters in support of the existence of an Fe–Fe single bond in each dimer (rather than the previously rejected alternative[8] that the diamagnetic behavior of these neutral complexes is a consequence of a weak spin–spin exchange and/or superexchange via the bridging ligands) due to the occupation of the strongly bonding $5a_1$ MO but not of its antibonding counterpart. For $Fe_2(CO)_6S_2$ the Fe–Fe stretching force constant of 1.3 ± 0.2 mdyn/Å,[25] deduced from a vibrational analysis of its Raman and infrared spectra, is not unexpected for an Fe–Fe bond order of 1. The electronic absorption peak at 335 nm and its shoulder at ca. 460 nm[26] may also be correlated with the electronic transitions from the six energetically similar iron "lone-pair" orbitals (except the $2b_1$ which is not allowed) and the HOMO ($5a_1$), respectively, to the LUMO ($4b_2$).

(b) Different Bonding Modes for the Bridging Ligands. Our selection of the particular Fe_2B_2-bridged systems (B = N, P, S) presented here was made in order to detect and correlate variations in the bonding of the Fe_2B_2 cores upon changes in the nature of the bridging ligands (i.e., those with and without direct B–B bonds and possessing widely differing electronegativities). The orbital populations of these ligand orbitals are listed in Table V, and the final MO's containing substantial bridging ligand character are tabulated in Table VI. In free *cis*-$CH_3N{=}NCH_3$ of C_{2v} geometry there are four MO's capable of interaction with the appropriate metal orbitals—viz., the two symmetrized lone-pair-type orbitals localized more or less on the nitrogen atoms (i.e., designated $5a_1$ and $4b_1$ which are symmetrical and antisymmetrical, respectively, with respect to the mirror plane that bisects the free ligand),[27,28] the filled bonding π orbital ($2b_2$), and the low-lying virtual, antibonding π^* orbital ($2a_2$). In $Fe_2(CO)_6(NCH_3)_2$, the interactions between the bridging *cis*-$CH_3N{=}NCH_3$ ligand and the iron atoms occur via the following routes (Table V): (1) a 0.74 electron donation from the high-lying antisymmetrical lone-pair ligand combination ($4b_1$) to the iron atoms; (2) a smaller donation of 0.20 electron from the symmetrical lone-pair ligand combination, $5a_1$; (3) a substantial back-bonding of 0.96 electron into the low-lying virtual antibonding

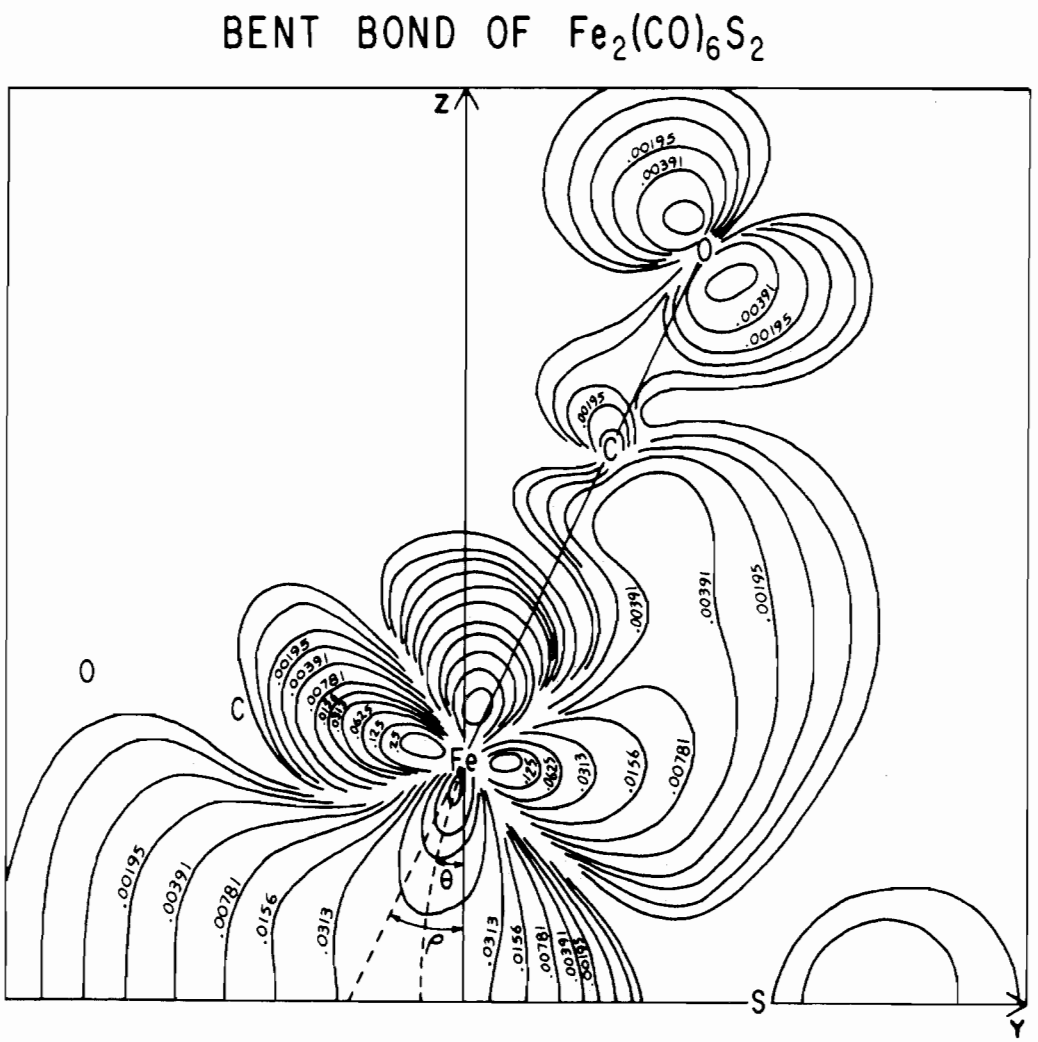

Figure 3. Electron density contour map in atomic units for the HOMO of $Fe_2(CO)_6S_2$ in the *yz* plane containing one symmetry-related iron atom, its axial carbonyl ligand, and the midpoint of the sulfur atoms. The vector between the two Fe atoms lies along the *z* axis with a two-fold axis coincident with the *y* axis and one mirror plane (passing through the two sulfur atoms and the midpoint of the two iron atoms) containing the *y* axis and perpendicular to the *z* axis. The angle θ between the tangent at the iron site of the contour of maximum electron density and the Fe-Fe vector was obtained (cf. Table IV) for comparison with the angle ρ between the Fe-Fe and Fe-CO(axial) vectors.

ligand π^* orbital, $2a_2$; and (4) a donation of 0.45 electron from the bonding π ligand orbital $2b_2$. Whereas the donation from the $4b_1$ ligand orbital strengthens the N–N bond, the donations from the $5a_1$ and $2b_2$ ligand orbitals and the back-donation into the $2a_2$ virtual orbital weaken the N–N bond. The net result is a weakening of the N–N bond as reflected in a drop of overlap population of about 20% (from 1.070 in free *cis*-azomethane to 0.894 in the complex, both being calculated at the same N–N distances) between the two nitrogen atoms. This is also in accord with the increase in nitrogen–nitrogen distance from a double-bond value of 1.24 Å[29] to the observed value of 1.37 Å[4a] in $Fe_2(CO)_6(NCH_3)_2$.

A somewhat different situation arises in $Fe_2(CO)_6S_2$. The valence electronic configuration of free S_2 is calculated at the iron-complexed S–S distance of 2.01 Å to be $(1\sigma_g)^2(1\sigma_u)^2(1\pi_u)^4(2\sigma_g)^2(1\pi_g)^2$. While the MO diagram (Figure 2) suggests that five ligand orbitals (viz., the doubly degenerate bonding $1\pi_u$ and doubly degenerate antibonding $1\pi_g$ orbitals and the symmetrical $2\sigma_g$ combination of the "lone pairs") are energetically accessible for iron–sulfur interactions, the orbital occupancies reveal that only the $1\pi_u$ and $1\pi_g$ ligand orbitals interact substantially with the valence iron orbitals (primarily due to the unfavorable orbital overlap between the $2\sigma_g$ and iron orbitals). The resulting Mulliken populations (Table V) of 3.41 for $1\pi_u$ and 2.27 for $1\pi_g$ correspond to a donation of 0.59 electron from the disulfur ligand to the iron atoms and a small back-bonding of 0.27 electron in the opposite direction. This suggests a weakening of the sulfur–sulfur bond with respect to the free S_2 group in accord with the observed S–S bond length of 2.01 Å in $Fe_2(CO)_6S_2$ being between the double-bond value of 1.89 Å and the single-bond value of 2.08 Å.[30,31]

The free radicals NH_2 and PH_2 are similar in character. In both cases the odd electron resides in the pure p_y HOMO ($1b_2$) perpendicular to the molecular plane. The highest doubly occupied MO ($2a_1$) corresponds to the "classical lone electron pair" on the trigonally hybridized nitrogen (or phosphorus), though it is somewhat bonding between the nitrogen (or phosphorus) and hydrogen atoms. Each NH_2 or PH_2 group thereby affords two orbitals ($2a_1$ and $1b_2$) and three electrons for its linkage to the two metal atoms. In $Fe_2(CO)_6(NH_2)_2$ each NH_2 ligand donates 0.54 electron through its lone pair ($2a_1$) and accepts 0.43 electron through its p_y ($1b_2$) orbital.

If an idealized C_{3v} geometry is assumed for the SCH_3 radical, the highest three occupied MO's are $3a_1$ and 2e, which correspond in the valence-bond model to the one "lone electron pair", and two p orbitals, respectively. These three orbitals, populated with five electrons, are mainly responsible for the bonding of each SCH_3 ligand to the two iron atoms. The

Table V. Bridging Ligand Orbital Occupancies

$Fe_2(CO)_6(NCH_3)_2$	$2a_2$	0.96
	$4b_1$	1.26
	$5a_1$	1.80
	$2b_2$	1.55
$Fe_2(CO)_6(NH_2)_2$	$1b_2$	1.43
	$2a_1$	1.46
$Fe_2(CO)_6S_2$	$1\pi_g$	x 1.16
		y 1.11
	$2\sigma_g$	2.00
	$1\pi_u$	x 1.79
		y 1.62
anti-$Fe_2(CO)_6(SCH_3)_2$	2e	x 1.67
		y 1.36
		(x 1.62)[a]
		(y 1.38)[a]
	$3a_1$	1.80
		(1.83)[a]
syn-$Fe_2(CO)_6(SCH_3)_2$	2e	x 1.63
		y 1.38
	$3a_1$	1.82
$Fe_2(CO)_6(PH_2)_2$	$3a_1$	0.01
	$2b_1$	0.07
	$1b_2$	1.22
	$2a_1$	1.36
$[Fe_2(CO)_6(PH_2)_2]^-$	$3a_1$	0.02
	$2b_1$	0.09
	$1b_2$	1.19
	$2a_1$	1.38
$[Fe_2(CO)_6(PH_2)_2]^{2-}$	$3a_1$	0.04
	$2b_1$	0.11
	$1b_2$	1.16
	$2a_1$	1.38

[a] Numbers in parentheses are due to the orbital occupancies of the two bridging ligands not being equal.

present calculations for the equatorial–axial anti or biaxial syn isomers[3b,32] of $Fe_2(CO)_6(SCH_3)_2$ showed no real differences in bonding except for a slight destabilization of the HOMO (ca. 0.3 eV) and a somewhat larger splitting of the two $3a_1$ lone pairs in the dimer in going from the anti to the syn configuration. A considerable redistribution of the electronic charge in $Fe_2(CO)_6(SCH_3)_2$ compared to that of the isolated SCH_3 ligands is indicated by the extensive participation of all six ligand orbitals, three on each SCH_3, in the Fe–S bonding which resulted in a net donation of 0.17 electron from each SCH_3 to the iron atoms.

It is noteworthy that the net donation of 0.43 electron by the *cis*-$CH_3N{=}NCH_3$ ligand to the two iron atoms in $Fe_2(CO)_6(NCH_3)_2$ is significantly higher than the corresponding net donation of only 0.22 electron by the two NH_2 ligands in $Fe_2(CO)_6(NH_2)_2$. In contrast, the net donation of 0.32 electron to the iron atoms by the S_2 ligand in $Fe_2(CO)_6S_2$ is similar to the net donation of 0.34 electron by the two SCH_3 ligands in $Fe_2(CO)_6(SCH_3)_2$. This smaller net electron donation results in each bridging nitrogen atom in $Fe_2(CO)_6(NH_2)_2$ possessing a small negative charge of −0.12 electron in contrast to each of the bridging atoms in the other dimers bearing a small positive charge—viz., $N^{0.09+}$ in $Fe_2(CO)_6(NCH_3)_2$, $S^{0.14+}$ in $Fe_2(CO)_6S_2$, and $S^{0.15+}$ in $Fe_2(CO)_6(SCH_3)_2$. These values are in sharp distinction to the formal charge of 1− usually assigned to each of these B atoms in the Fe_2B_2-bridged dimers.

(c) Structural and Electronic Interrelationship of Fe_2B_2 Cores with and without B–B Bonds. From a detailed comparison of the corresponding molecular parameters of several nitrogen-bridged diiron hexacarbonyl complexes which possess N–N bonds with those which have no direct N–N linkages, Doedens[4a-c] observed that there were highly significant differences in the Fe–Fe and Fe–N bond lengths and Fe–N–Fe bond angles. The (N–N)-bonded iron carbonyl dimers including $Fe_2(CO)_6(NCH_3)_2$ were found to have, relative to their (N···N)-nonbonded counterparts including $Fe_2(CO)_6(NH_2)_2$, (1) *longer* electron-pair Fe–Fe distances of range 2.49–2.53 Å vs. those of range 2.37–2.42 Å, (2) *shorter* Fe–N bond lengths of range 1.88–1.92 Å vs. ones of range 1.97–2.02 Å, (3) *larger* Fe–N–Fe bond angles of 81–83° vs. those of 72–75°. A comparison of the corresponding molecular parameters between $Fe_2(CO)_6S_2$ and $Fe_2(CO)_6(SC_2H_5)_2$ (Table I) shows that the differences are in the same direction as for the two types of Fe_2N_2-bridged dimers but are considerably smaller in magnitude (to such an extent as to be either marginally or not significantly different). This correlation of a *longer* Fe–Fe bond being associated with a *shorter* Fe–B bond was first noted by Weber and Bryan[3j] for the Fe_2S_2-bridged dimers from their X-ray study of $Fe_2(CO)_6(S_2C_2(C_6H_5)_2)$ and was later clearly illustrated (because of the much larger and significant bond-length differences) by Doedens[4a-c] for the Fe_2N_2-bridged dimers.

The basis of this observed *increase* of the Fe–Fe bond lengths by ca. 0.10 Å with a concomitant *decrease* of the mean Fe–N bond lengths by a comparable amount in the Fe_2N_2 cores of the (N–N)-bonded iron carbonyls relative to the Fe_2N_2 cores of their (N···N)-nonbonded analogs has been ascribed by Doedens[4a-c] as stereochemical consequences stemming from strain effects at the bridging nitrogen atoms in their resistance to large deformations from a tetrahedral-like configuration.

The molecular orbital calculations not only provide a rationale for the above crystallographic results but also emphasize the importance of orbital overlap considerations as well as orbital energetics in affecting changes in molecular geometry. For convenience in describing the metal–ligand interactions relative to an analysis of the Fe–B and Fe–Fe interactions in terms of orbital overlap populations for the two types of Fe_2N_2-bridged dimers and Fe_2S_2-bridged dimers, the valence orbitals of the bridging ligands are classified as in plane or out of plane depending upon whether they are symmetric or antisymmetric with respect to the mirror plane perpendicular to the Fe–Fe vector and passing through the two bridging B atoms. It follows that there are two relevant in-plane ligand orbitals for the dimer with either two NH_2 or two PH_2 ligands (viz., two $2a_1$), with $X_2 = (NCH_3)_2$ (viz., $5a_1$ and $4b_1$) or with $X_2 = S_2$ (viz., the x components of $1\pi_u$ and of $1\pi_g$), and likewise two relevant out-of-plane ligand orbitals for the dimer with X = NH_2 or PH_2 (viz., two $1b_2$), with $X_2 = (NCH_3)_2$ (viz., $2b_2$ and $2a_2$) or with $X_2 = S_2$ (viz., the y components of $1\pi_u$ and of $1\pi_g$).

Our model conceptually assumes each of the NH_2 radicals in $Fe_2(CO)_6(NH_2)_2$ to interact partially through its in-plane sp^2-like lone-pair orbital with a symmetrical combination (relative to the mirror plane passing through the nitrogen atoms) of iron orbitals and partially through the out-of-plane half-filled p orbital (perpendicular to the NH_2 plane) with an antisymmetrical diiron combination. On the other hand, the mode of Fe–N interaction in $Fe_2(CO)_6(NCH_3)_2$ may be envisioned to occur via a direct donation from the in-plane symmetrical $5a_1$ and antisymmetrical $4b_1$ lone-pair ligand orbitals into symmetrical diiron combinations and from a filled π orbital ($2b_2$) into an antisymmetrical diiron combination together with back-bonding from a filled antisymmetrical diiron combination into the low-lying virtual π^* ligand orbital ($2a_2$). Hence, in both types of nitrogen-bridged molecules, to the extent that iron–iron orbital interactions occur indirectly through the multicenter Fe–N interactions, an *enhancement* of the Fe–N interactions involving the in-plane lone-pair nitrogen orbitals will add *bonding* character between the two iron atoms but a similar Fe–N *enhancement* involving the out-of-plane nitrogen orbitals will produce Fe–Fe *antibonding* character.

Unfavorable in-plane Fe–N orbital overlap in $Fe_2(C-$

Table VI. Percent Character and Energy of Some Filled Orbitals Containing Substantial Bridging Ligand Character

Energy, eV	Orbital[a]	Orbitals on each Fe atom	Bridging ligand orbital
		$Fe_2(CO)_6(NCH_3)_2$	
−11.85	$1a_2$	d_{xy} (13.3), p_x (9.3)	$2a_2$ (47.2)
−15.42	$1b_1$	d_{xy} (6.0), d_{xz} (3.9), p_x (6.7)	$4b_1$ (58.8)
−17.09	$2a_1$	d_{yz} (2.4), p_y (3.8), d_{z^2} (1.6)	$5a_1$ (64.7)
−17.60	$1a_1$	d_{z^2} (9.5), p_z (4.0)	$5a_1$ (17.4)
−18.14	$2b_2$	d_{z^2} (1.2), $d_{x^2-y^2}$ (1.4), p_y (6.1)	$2b_2$ (28.2)
−19.16	$1b_2$	d_{z^2} (1.2), s (5.4)	$2b_2$ (43.1)
		$Fe_2(CO)_6(NH_2)_2$	
−14.21	$1b_2$	d_{z^2} (2.4), p_y (7.7), s (1.1)	$1b_2$ (2 × 34.3)[b]
−14.47	$1a_2$	d_{xy} (8.1), p_x (5.6)	$1b_2$ (2 × 34.3)
−17.24	$2b_1$	d_{xy} (1.1), d_{xz} (2.5), p_x (9.6)	$2a_1$ (2 × 12.2)
−17.66	$1b_1$	d_{xy} (17.6)	$2a_1$ (2 × 20.9)
−18.48	$2a_1$	d_{z^2} (2.9), d_{yz} (2.3), p_y (5.2), p_z (2.2)	$2a_1$ (2 × 24.4)
−19.08	$1a_1$	s (6.3)	$2a_1$ (2 × 9.5)
		$Fe_2(CO)_6S_2$	
−11.55	$1a_2$	d_{xy} (11.6), p_x (7.2)	$1\pi_g y$ (54.6)
−11.86	$1b_1$	d_{xy} (9.6), d_{xz} (9.3), p_x (2.7)	$1\pi_g x$ (48.3)
−14.61	$2a_1$	$d_{x^2-y^2}$ (2.2)	$2\sigma_g$ (89.8); $1\pi_u x$ (4.0)
−15.62	$1a_1$	d_{yz} (3.2), p_y (3.8)	$1\pi_u x$ (77.0)
−15.68	$1b_2$	d_{z^2} (2.6), p_y (6.2)	$1\pi_u y$ (72.4)
		anti-$Fe_2(CO)_6(SCH_3)_2$	
−11.62	4a′	$d_{x^2-y^2}$ (2.9), d_{yz} (2.5), p_x (1.5)	$2e_x$ (58.4, 4.5); $3a_1$ (6.4, 10.0)[c]
−12.46	3a′	d_{xy} (4.0), d_{xz} (3.5), d_{yz} (2.6)	$2e_x$ (3.0, 57.8); $3a_1$ (0.3, 4.6)
−12.84	2a″	d_{xy} (11.1), p_x (4.3)	$2e_y$ (44.9, 18.3)
−13.11	1a″	d_{z^2} (3.0), p_y (7.7)	$2e_y$ (18.4, 46.1)
−16.31	2a′	d_{xy} (10.9), p_y (1.8)	$3a_1$ (47.1, 4.1)
−17.09	1a′	d_{z^2} (1.3), p_x (2.6), p_y (2.2)	$3a_1$ (0.0, 57.0)
		syn-$Fe_2(CO)_6(SCH_3)_2$	
−12.25	$2b_1$	d_{xy} (4.8), d_{xz} (5.5)	$2e_x$ (2 × 29.7)
−12.74	$2a_1$	$d_{x^2-y^2}$ (1.3), d_{yz} (6.6), p_y (1.9)	$2e_x$ (2 × 33.4)
−12.85	$1a_2$	d_{xy} (11.3), p_x (4.6)	$2e_y$ (2 × 31.9)
−13.15	$1b_2$	d_{z^2} (3.2), p_y (7.9)	$2e_y$ (2 × 32.5)
−15.34	$1b_1$	d_{xy} (5.9), p_x (4.7)	$3a_1$ (2 × 35.5)
			$2e_x$ (2 × 2.0)
−18.16	$1a_1$	p_y (4.1)	$3a_1$ (2 × 34.0)
		$Fe_2(CO)_6(PH_2)_2$	
−12.24	$1a_2$[d]	d_{xy} (15.4), p_x (4.7)	$1b_2$ (2 × 26.6)
−12.75	$1b_2$	d_{z^2} (3.7), p_y (9.8)	$1b_2$ (2 × 27.5)
−14.35	$1b_1$	d_{xy} (17.9), d_{xz} (1.7), p_x (4.2)	$2a_1$ (2 × 24.0)
−16.80	$3a_1$	d_{yz} (2.3), p_y (10.2)	$2a_1$ (2 × 23.6)
−17.39	$2a_1$	d_{z^2} (10.0), p_z (5.4)	$2a_1$ (2 × 4.0)
−19.10	$1a_1$	s (4.4)	$2a_1$ (2 × 7.9)
		$[Fe_2(CO)_6(PH_2)_2]^-$[e]	
−12.14	$1a_2$	d_{xy} (18.4), p_x (3.7)	$1b_2$ (2 × 25.1)
−13.00	$1b_2$	d_{z^2} (2.4), s (1.0), p_y (11.6)	$1b_2$ (2 × 26.3)
−13.36	$1b_1$	d_{xy} (18.5), d_{xz} (1.5), p_x (4.4)	$2a_1$ (2 × 23.4)
−17.04	$3a_1$	d_{z^2} (5.3), p_y (6.2), p_z (2.1)	$2a_1$ (2 × 5.4)
−17.29	$2a_1$	d_{z^2} (4.1), p_y (3.5), p_z (3.9)	$2a_1$ (2 × 21.6)
−19.12	$1a_1$	s (4.8)	$2a_1$ (2 × 11.2)
		$[Fe_2(CO)_6(PH_2)_2]^{2-}$[e]	
−11.92	$1a_2$	d_{xy} (21.4), p_x (2.5)	$1b_2$ (2 × 22.8)
−12.00	$1b_1$	d_{xy} (19.4), p_x (5.6)	$2a_1$ (2 × 21.7)
−13.40	$1b_2$	d_{z^2} (1.5), s (1.2), p_y (12.8), p_z (1.3)	$1b_2$ (2 × 24.8)
−17.87	$1a_1$	p_y (7.4)	$2a_1$ (2 × 22.8)

[a] Symmetry representation numbering is concerned only with molecular orbitals containing mainly bridging ligand or metal character. [b] 2 times a number in parentheses implies that two separate ligands have the same percent character. [c] Two numbers in parentheses imply that the contributions from the two bridging ligands are not equal. [d] For the purpose of comparison, orbital symmetry representations for $[Fe_2(CO)_6(PH_2)_2]^n$ series are made to be analogous. [e] The orbital energies of the mono- and dianions of $Fe_2(CO)_6(PH_2)_2$ have been shifted by −4.75 and −9.50 eV, respectively, to place the nonbonding CO 3σ levels on the same scale as that in the neutral species.

$O)_6(NCH_3)_2$ relative to that in $Fe_2(CO)_6(NH_2)_2$ is presumed to contribute largely to a shortening of the Fe–N bonds (to optimize the Fe–N interactions) and concomitantly to a lengthening of the Fe–Fe bond with respect to those in $Fe_2(CO)_6(NH_2)_2$. This is readily seen in Figure 4 which depicts the two in-plane lone-pair nitrogen orbitals in an $Fe_2(CO)_6(NR)_2$ dimer being oriented in an outward direction while the two in-plane nitrogen orbitals of the NR_2 ligands in an $Fe_2(CO)_6(NR_2)_2$ dimer point more nearly toward the midpoint of the two iron atoms. Hence, a much better Fe–N bonding interaction is expected at equivalent Fe–N distances for the Fe_2N_2-bridged dimers with no N–N bonds. Overlap populations support this premise in that for $Fe_2(CO)_6(NH_2)_2$ the Fe–N contributions from the in-plane and out-of-plane nitrogen orbitals are similar (viz., 0.17 and 0.21 electron), whereas for $Fe_2(CO)_6(NCH_3)_2$ the Fe–N overlap population from the in-plane nitrogen orbitals is reduced to about half (0.09 electron) of the corresponding value of 0.22 electron from the out-of-plane nitrogen orbitals. This would suggest a weakening of the Fe–N bonds in going from (N···N)-

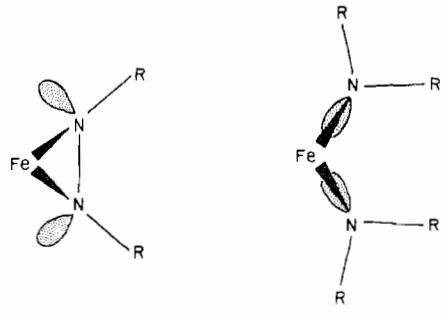

Figure 4. Orientation of the two in-plane lone-pair nitrogen orbitals of a *cis*-RN=NR bridging ligand in an $Fe_2(CO)_6(NR)_2$ dimer and of the corresponding two NR_2 bridging ligands in an $Fe_2(CO)_6(NR_2)_2$ dimer. The views are each normal to the mirror plane passing through the bridging ligands and the midpoint of the Fe–Fe vector and thereby superimposing the two mirror-related iron atoms on each other.

nonbonded to (N–N)-bonded Fe_2N_2 dimers which, on account of the mean Fe–N bond length in $Fe_2(CO)_6(NH_2)_2$ being 0.10 Å *larger* than that in $Fe_2(CO)_6(NCH_3)_2$, at first glance appears to be incompatible with the widely assumed notion that a shorter distance is associated with a stronger bond. However, this comparison again emphasizes that an inverse distance–bond strength relationship does not necessarily hold for *different* geometries. In fact, if the present calculations were performed at identical Fe–N distances for both kinds of corresponding dimers rather than at their observed equilibrium distances, an even larger disparity in Fe–N overlap population would be obtained. Hence, we propose that the shortening of the Fe–N bonds by 0.10 Å in going from (N···N)-nonbonded to (N–N)-bonded dimers is an attempt to compensate for a weakening of the Fe–N bonding due to unfavorable Fe–N-(in-plane) orbital overlap. Since the in-plane and out-of-plane nitrogen orbitals interact with the bonding and antibonding diiron symmetry combinations, respectively, the much smaller Fe–N(in-plane) overlap population cited above for $Fe_2(CO)_6(NCH_3)_2$ compared to that for $Fe_2(CO)_6(NH_2)_2$ indicates a smaller indirect bonding contribution to the Fe–Fe overlap population in an (N–N)-bonded dimer. This effect coupled with a 0.10 Å longer Fe–Fe distance, which we regard as a geometrical consequence of the Fe–N bond shortening, is presumed to account for the overlap population between the Fe–Fe atoms of 0.06 electron in $Fe_2(CO)_6(NCH_3)_2$ being less than that of 0.14 electron in $Fe_2(CO)_6(NH_2)_2$.

An analysis of the corresponding Fe–S and Fe–Fe overlap populations in $Fe_2(CO)_6S_2$ and $Fe_2(CO)_6(SCH_3)_2$ shows a similarly low contribution to the overlap population from the Fe–S(in-plane) interactions of 0.08 electron compared to the Fe–S(out-of-plane) ones of 0.19 electron in $Fe_2(CO)_6S_2$ in contrast to the similar Fe–S(in-plane) and Fe–S(out-of-plane) interactions of 0.17 and 0.20 electron, respectively, in $Fe_2(CO)_6(SCH_3)_2$. However, the Fe–Fe overlap populations of 0.10 electron in $Fe_2(CO)_6S_2$ and 0.11 electron in $Fe_2(CO)_6(SCH_3)_2$ are virtually identical. We attribute these results to be in accord with the much smaller variations found in the Fe–S and Fe–Fe bond lengths between the two Fe_2S_2 cores. The fact that the Fe–B(in-plane) orbital overlap is more favorable with the bridging S_2 ligand than with the electronically equivalent *cis*-$(NCH_3)_2$ ligand leads to similar Fe–B overlap populations without the necessity in the S_2-bridged dimer of an extensive decrease in the Fe–S distances together with a compensatory increase in the Fe–Fe distance.

The $[Fe_2(CO)_6(PH_2)_2]^n$ Complexes (n = 0, 1–, 2–). (a) General Remarks. In order to investigate the electronic effects produced by a reduction of the $Fe_2(CO)_6X_2$ complexes for the purpose of correlating the extensive spectroscopic data obtained by Dessy and coworkers[7] for the dimethylphosphido-bridged iron carbonyl anions, MO calculations were performed on the series $[Fe_2(CO)_6(PH_2)_2]^n$ (n = 0, 1–, 2–). The bonding of this model series will be discussed along with the experimental observations which hopefully will provide chemical insight of some generality for other analogous series.

(b) Redox Properties and Stereochemical Variation. The MO energy diagrams for $[Fe_2(CO)_6(PH_2)_2]^n$ (n = 0, 1–, 2–) are portrayed in Figure 5. The absolute values of the energy levels resulting from these MO calculations for the charged species differed substantially from those of the neutral precursor due to a lack of stabilization by counterions. In order to provide a comparison of the relative trends of the eigenvalues of these anions to those of the parent molecule, the eigenvalues of the 1– and 2– charged species were standardized to the lowest valence carbonyl 3σ orbital combination, which may be assumed not to be appreciably affected by the stereochemical or charge changes. This linear scaling of the energy levels to obtain identical 3σ carbonyl levels amounted to a stabilization of the monoanion by 4.75 eV and of the dianion by 9.50 eV.

An examination of these appropriately scaled MO diagrams revealed the following features. The neutral species has a low-lying virtual orbital (LUMO) of predominantly antibonding metal character at 3.9 eV above the HOMO (which is also principally associated with the metal orbitals), in close resemblance to the orbital character of the LUMO's and HOMO's of the two neutral sulfur- and two neutral nitrogen-bridged species (vide supra). Due to its highly *antibonding metallic* character, a stepwise addition of one or two electrons to this LUMO $4b_2$ orbital via reduction should cause a stepwise increase in the metal–metal distance from that of a two-electron bond (for n = 0), to that of a "net" one-electron bond (for n = 1–), to a "net" nonbonding value (for n = 2–). Although no crystallographic data are as yet known for these $Fe_2(CO)_6X_2$ anions, the reported spectroscopic data[7] are in complete harmony with this premise. The injection of one or two electron(s) into this low-lying $4b_2$ orbital produces no drastic reordering of the energy levels relative to one another (as indicated from Figure 5 and Tables III and VI) other than the expected sharp drop of the $4b_2$ level upon occupancy due mainly to the assumed marked increase in Fe–Fe distance associated with its strongly antibonding diiron character. At the nonbonding Fe···Fe distance of 3.36 Å assumed for the dianion, the $4b_2$ and $6a_1$ are almost degenerate as a result of their being effectively nonbonding with respect to the two iron atoms. However, a significant electron redistribution does occur upon reduction of the phosphido-bridged dimer as evidenced from the following correlations of the MO results with the available spectral data.

(c) EPR Characterization of the LUMO. From the EPR spectrum of the $[Fe_2(CO)_6(P(CH_3)_2)_2]^-$ radical anion showing hyperfine interactions involving the phosphorus nuclei and six of the twelve methyl protons, but no evidence for hyperfine interactions involving the carbonyl carbons, Dessy and coworkers[7a] initially suggested that the spin density resides largely, if not wholly, in the dimethylphosphido ligands. In complete contrast, the model calculation of the $[Fe_2(CO)_6(PH_2)_2]^-$ radical anion gives 80% metal, 1% bridging ligand, and 14% carbonyl character for the singly occupied $4b_2$ MO. The small magnitude of the bridging ligand orbital character calculated for the orbital containing the unpaired electron in the PH_2-bridged dimer compared to the larger bridging ligand character needed to account for the EPR data of the $P(CH_3)_2$-bridged dimer is deemed to arise from a composite of the following factors: (1) an exclusion of the virtual phosphorus 3d orbitals from the calculations, (2) an uncertainty in the anion's stereochemistry, and (3) a significant difference caused by replacement of the methyl substituents

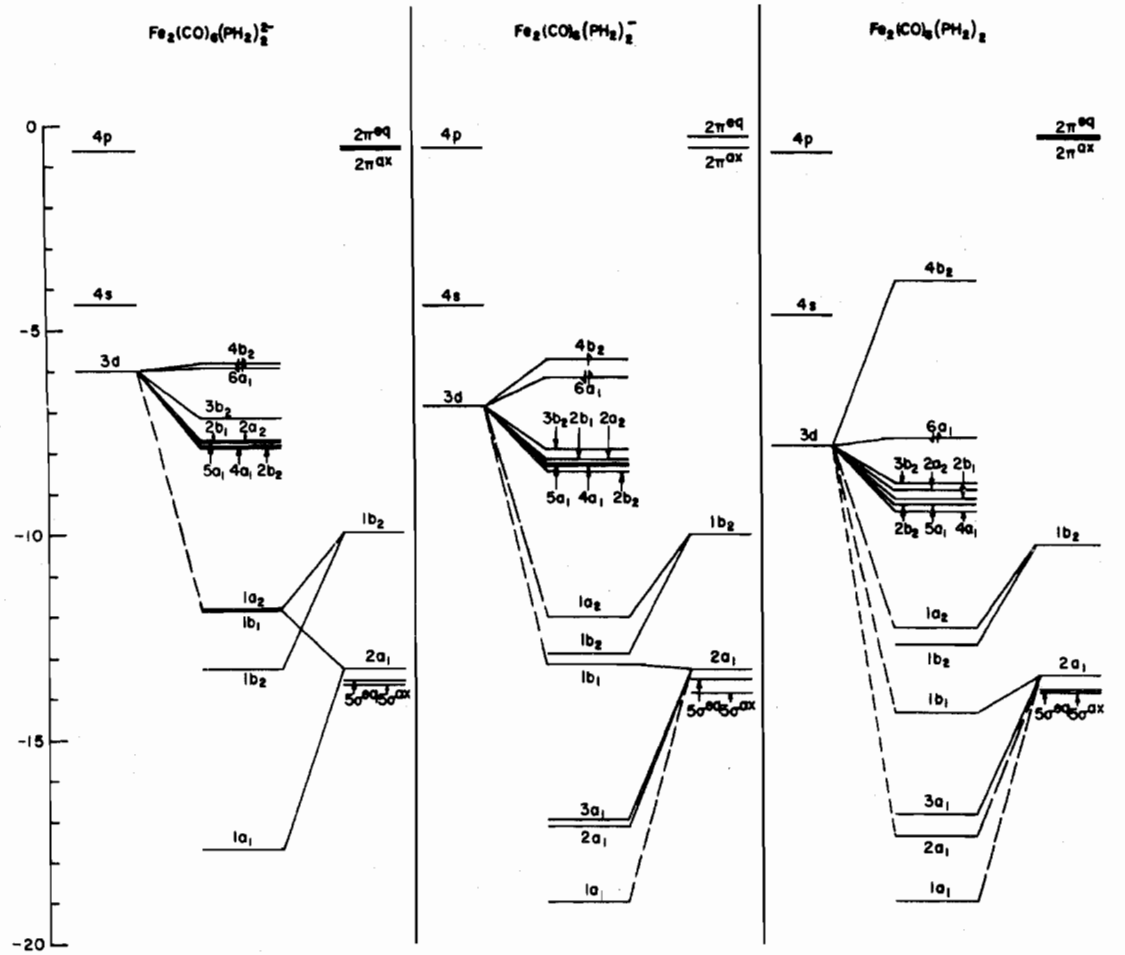

Figure 5. Molecular orbital energy diagrams for the series $[Fe_2(CO)_6(PH_2)_2]^n$ where $n = 0, 1-, 2-$.

Table VII. Electronic Configuration of Metal Atoms in $[Fe_2(CO)_6(PH_2)_2]^n$

Complex	$3d_{z^2}$	$3d_{xy}$	$3d_{x^2-y^2}$	$3d_{xz}$	$3d_{yz}$	4s	$4p_x$	$4p_y$	$4p_z$
$Fe_2(CO)_6(PH_2)_2$	1.16	1.11	1.58	1.56	1.43	0.29	0.49	0.46	0.50
$[Fe_2(CO)_6(PH_2)_2]^-$	1.29	1.10	1.54	1.50	1.47	0.28	0.50	0.48	0.59
$[Fe_2(CO)_6(PH_2)_2]^{2-}$	1.44	1.11	1.48	1.43	1.50	0.28	0.52	0.48	0.68

with hydrogen atoms (i.e., since the LUMO is of b_2 representation, it cannot acquire hydrogen 1s orbital character for a bridging PH_2 ligand due to the orbital symmetry, whereas for $P(CH_3)_2$ it can acquire some methyl substituent character). Since the compositions of the corresponding LUMO's in the neutral nitrogen- or sulfur-bridged molecules with methyl substituents consist of 6–10% bridging orbital character, we conclude that such a range is in complete accord with the EPR spectrum of the $[Fe_2(CO)_6(P(CH_3)_2)_2]^-$ radical anion exhibiting a 1:2:1 triplet with a hyperfine coupling of 4.5 G due to two equivalent phosphorus nuclei together with a further sevenfold hyperfine splitting of each triplet member by 1.4 G due to one set of six equivalent methyl protons.

There is no experimental evidence for the composition of the HOMO in $Fe_2(CO)_6(P(CH_3)_2)_2$ or any of the other $Fe_2(CO)_6X_2$ molecules. However, the structurally analogous and electronically equivalent $Co_2(\eta^5\text{-}C_5H_5)_2(P(C_6H_5)_2)_2$ molecule[8] was found[33] to undergo a one-electron oxidation to yield the radical cation which shows at room temperature a well-resolved 31-hyperfine-line EPR spectrum. This can be interpreted on the basis of a splitting into 15 lines of intensitites 1:2:3...8...3:2:1 due to two equivalent cobalt nuclei ($I = {}^7/_2$ for ^{59}Co, 100%) with a hyperfine constant $a_{Co} = 22.66$ G with each of these lines further split into a 1:2:1 triplet with $a_P = 11.33$ G due to two equivalent phosphorus nuclei ($I = {}^1/_2$). This spectrum was semiquantitatively analyzed to yield a total of 50% spin density on the two cobalt atoms, 8.5% spin density on the two phosphorus atoms, and the rest presumably delocalized over the cyclopentadienyl as well as phenyl groups.[33] This percent orbital character of the singly occupied HOMO is in harmony with our calculations on the neutral $Fe_2(CO)_6X_2$ analogs that the filled HOMO's are primarily metal in character.

(d) Mössbauer Evidence of Charge Distribution and Electronic Configuration. Since the isomer shift (δ) of the Mössbauer spectra is a measure of the total s electron density at the nucleus, while the nuclear quadrupole splitting (Δ) is a measure of the deviation of the electronic charge surrounding the nucleus from spherical symmetry, a qualitative correlation is expected between our calculated charge distributions and the Mössbauer parameters reported[7a] for $[Fe_2(CO)_6(P(CH_3)_2)_2]^n$ ($n = 0, 1-, 2-$).

A comparison of the charges and electronic configuration of the metal atoms in the neutral and anionic species (Tables VII and VIII) indicates no unexpected or drastic changes except for a small increase in electronic charge in going from N to S to P. However, the bridging atoms (Table IX) exhibit a steady increase in positive charge in going from N to S to P. To a large extent, this trend can be attributed to the decrease in electronegativity in the order N > S > P.[34]

The assumed $3d^7$ Fe^+ electronic configuration (based upon formal oxidation states) for each of the two iron atoms in the

Table VIII. Electronic Configuration, Mulliken Gross Atomic Charge, and Mössbauer Isomer Shift for Each Iron Atom in $[Fe_2(CO)_6X_2]^n$

Complex	3d	4s	4p	Charge[a]	Charge (3d)[b]	δ,[c] mm/sec
$Fe_2(CO)_6(NCH_3)_2$	6.71	0.35	1.35	0.41–	1.29	
$Fe_2(CO)_6(NH_2)_2$	6.68	0.36	1.28	0.31–	1.32	
$Fe_2(CO)_6S_2$	6.79	0.30	1.28	0.36–	1.21	
anti-$Fe_2(CO)_6(SCH_3)_2$	6.78	0.30	1.31	0.39–	1.22	0.28[d]
syn-$Fe_2(CO)_6(SCH_3)_2$	6.77	0.31	1.31	0.39–	1.23	0.285[d]
$Fe_2(CO)_6(PH_2)_2$	6.84	0.29	1.44	0.57–	1.16	0.25[e]
$[Fe_2(CO)_6(PH_2)_2]^-$	6.90	0.28	1.56	0.74–	1.10	0.19[e]
$[Fe_2(CO)_6(PH_2)_2]^{2-}$	6.96	0.28	1.69	0.93–	1.04	0.10[e]

[a] Mulliken gross atomic charge. [b] Mulliken gross atomic charge for 3d AO's only. [c] The arbitrary reference of zero is sodium nitroprusside ($Na_2Fe(CN)_5NO\cdot 2H_2O$). [d] Reference 36. [e] Reference 7a.

Table IX. Mulliken Gross Atomic Charges on Ligands in $[Fe_2(CO)_6X_2]^n$

	Carbonyl							
	Axial		Equatorial		Bridging Ligand[a]			
Complex	C	O	C	O	B	C	H	Total
$Fe_2(CO)_6(NCH_3)_2$	0.20	0.12–	0.20	0.12–	0.09	0.01	0.02	0.35
$Fe_2(CO)_6(NH_2)_2$	0.20	0.11–	0.20	0.11–	0.12–		0.08	0.07
$Fe_2(CO)_6S_2$	0.18	0.11–	0.19	0.12–	0.14			0.28
anti-$Fe_2(CO)_6(SCH_3)_2$	0.19	0.11–	0.21	0.12–	0.15[b]	0.08–	0.03	0.15
					0.16	0.09–	0.03	0.16
syn-$Fe_2(CO)_6(SCH_3)_2$	0.18	0.12–	0.21	0.13–	0.15	0.09–	0.03	0.16
$Fe_2(CO)_6(PH_2)_2$	0.20	0.13–	0.22	0.13–	0.53		0.10–	0.33
$[Fe_2(CO)_6(PH_2)_2]^-$	0.17	0.20–	0.19	0.21–	0.57		0.14–	0.30
$[Fe_2(CO)_6(PH_2)_2]^{2-}$	0.14	0.27–	0.16	0.28–	0.64		0.17–	0.30

[a] Calculated for S and P without inclusion of virtual 3d AO's. [b] The two sets of values are a consequence of the two SCH_3 ligands being nonequivalent which lowers the symmetry of the idealized molecular geometry from C_{2v}-2*mm* to C_s-*m* with the mirror plane passing through the two sulfur and two carbon atoms.

$Fe_2(CO)_6X_2$ molecules is consistent with the seven highest filled MO's (as well as the LUMO) in each neutral dimer being composed largely of 3d iron orbital character (cf. Figures 2 and 5 and Table III). An addition of one electron to a neutral dimer may then be expected to give rise either to a mixed-metal valency (integral oxidation states) of one $3d^8$ Fe^0 and one $3d^7$ Fe^+ or to two equivalent iron centers with an average $3d^{7.5}$ $Fe^{0.5+}$ corresponding to the delocalization MO model presented here. A Mössbauer spectrum of the monoanion at −196° shows no evidence of nonequivalent iron atoms thereby establishing that the two iron sites are structurally and electronically equivalent within a time scale of 10^{-7} sec (i.e., the electronic state lifetime for the existence of a distinct mixed Fe^0–Fe^+ valence state must be less than 10^{-7} sec).[35] An addition of two electrons should then similarly produce two $3d^8$ Fe^0. If there is no significant intramolecular charge redistribution upon reduction, we would then expect large changes in the Mossbauer isomer shift upon conversion of the parent compound to the mono- and dianions. However, the observed Mössbauer spectra[7a] at −196° for $[Fe_2(CO)_6(P(CH_3)_2)_2]^n$ (n = 0, 1−, 2−) reveal only *small* (but significant) negative isomer shifts from 0.25 mm/sec (relative to sodium nitroprusside) for n = 0 to 0.19 mm/sec for n = 1− to 0.10 mm/sec for n = 2−, thereby indicating a small increase in the overall s electron density at the iron nuclei; it is highly significant that these directional shifts are much smaller than that of ≥0.3 mm/sec expected for a change in isomer shift from Fe(I) to Fe(0).

This small variation in the Mössbauer isomer shifts observed among the $[Fe_2(CO)_6(P(CH_3)_2)_2]^n$ (n = 0, 1−, 2−) series, which indicates little alteration in the charge distribution of the iron atoms, could be taken as strong evidence that the electrons are added to a molecular orbital comprised mainly of bridging ligand orbitals.[7a] However, an examination of our calculated iron electronic configuration suggests that the isomer shift trend is a natural consequence of an electronic redistribution phenomenon common to reduced organometallic complexes[7b] involving a pronounced ability of the metal atoms to perform mainly as charge distributors in transmitting increased electron density mostly to the ligands, especially into the carbonyl electron sinks. In simple qualitative terms, this charge transmission arises due to the destabilization of the iron 3d orbitals upon successive reduction such that they become closer in energy to the carbonyl antibonding 2π orbitals and further removed from the carbonyl electron-donating 5σ orbitals. Thus, there is a net decrease in $5\sigma(CO) \rightarrow 3d(Fe)$ donation but a larger increase in $3d(Fe) \rightarrow 2\pi(CO)$ backdonation (cf. Table XI) in order to reduce effectively the unfavorably high negative charge on the metal atoms. Upon a stepwise reduction from n = 0 to 1− and from n = 1− to 2−, the d_{z^2} and p_z orbital occupancies (Tables VII and VIII) increase by ca. 0.15 and 0.10 electron, respectively, whereas each of the $d_{x^2-y^2}$ and d_{xz} orbital occupancies decreases by ca. 0.06 electron resulting in a net increase of only 0.12 electron in the total 3d orbital occupancy, no significant change in the 4s orbital occupancy, and a net increase of 0.25 electron in the 4p orbital occupancy. Hence, although the additional electron(s) in the anions occupy a molecular orbital that is highly antibonding with respect to the metal atoms, the metal atoms also act as *charge transmitters* such that the increased total electron density in the anions is dissipated essentially over the whole metal cluster system (especially into the carbonyl electron sinks) thereby rendering stable the negatively charged species. This phenomenon, not unexpected from the electroneutrality principle, is believed to be fairly general in metal carbonyl clusters, and therefore care must be taken in the assignment of formal oxidation states in these highly delocalized cluster systems.

The small observed decrease in the chemical isomer shift upon stepwise reduction of the dimethylphosphido-bridged dimer parallels the progressively lower values of chemical isomer shift observed[36b] for binary iron carbonyl species upon an increase in anionic charge from 0 to 1− to 2−. This isomer shift–charge trend in the iron carbonyl anions has been attributed by Greatrex and Greenwood[36b] to a combination of three major simultaneous interactions which increase the s electron density at an iron nucleus: (1) an increase in iron 4s orbital occupancy; (2) a decrease in iron 3d populations as

Table X. B···B Interactions for Fe_2B_2-Bridged Dimers without Direct B–B Bonds

Complex	B···B distance,[a] Å	Valence s(B)···s(B′) overlap[b]	In-plane $2a_1$(B)–$2a_1$(B′) overlap[c]	$2a_1$(B)–$2a_1$(B′) overlap population	Total B···B′ overlap population
$Fe_2(CO)_6(PH_2)_2$	2.86	0.0698	0.236	0.0139	0.0334
$[Fe_2(CO)_6(PH_2)_2]^-$	2.77	0.0816	0.278	0.0187	0.0463
$[Fe_2(CO)_6(PH_2)_2]^{2-}$	2.68	0.0951	0.344	0.0290	0.0622
$Fe_2(CO)_6(NH_2)_2$	2.50	0.0330	0.0949	−0.0038	−0.0087

[a] Table I. [b] Denotes overlap between the 3s AO's of the two bridging P atoms and between the 2s AO's of the two bridging N atoms. [c] Denotes overlap between the two in-plane sp^2-like lone-pair orbitals (labeled $2a_1$ for each of the "free" NH_2 or PH_2 ligands). Under molecular C_{2v} symmetry, two such orbitals produce symmetrical a_1 and antisymmetrical b_1 combinations which are both primarily involved in Fe–B bonding.

a result of increased 3d(Fe) → π*(CO) back-bonding (a deshielding effect); (3) a radial expansion of the nonbonding (i.e., non-s) electrons as a consequence of the progressive increase in anionic charge (a deshielding effect). However, our MO results for the $[Fe_2(CO)_6(PH_2)_2]^n$ series (Table VIII) do not show any increase in the 4s iron orbital occupancies but a stepwise increase in the 3d and 4p iron populations upon a variation in anionic charge from $n = 0$ to 1− to 2−, thereby predicting an increase in the shielding effect and hence a concurrent diminution in s electron density at each iron nucleus (in contrast to the *small increase* suggested by the isomer shifts of the dimethylphosphido-bridged series).

The inability of the Fenske–Hall treatment to correlate the calculated electronic configurations with the small changes in the Mössbauer isomer shift data of the phosphido-bridged dimers is not at all surprising in light of its inherent approximations (including the use of the Mulliken population analysis) coupled with the following considerations: (1) the freezing of all inner-shell core electrons (which have been shown to play an important role in dictating isomer shifts of iron compounds[36c]) as well as of all valence orbital radial functions in our calculations of the neutral and anionic dimers in order to minimize the possibility of any incorporation of preconceived correlations which may be fallacious; (2) the lack of a reliable theoretical treatment to estimate the magnitudes of individual contributions to the total s electron density at the iron nucleus;[36b] (3) the electron density which determines the isomer shift amounting to only 10^{-10} of the total density on the iron atom;[36b] (4) the neglect of electron correlation and relativistic effects. We conclude that orbital expansion[36b] as well as inner-shell overlap distortion effects[36c] may be important in dictating the Mössbauer isomer shifts of low-valency iron carbonyl species with varying charges.

The relatively small quadrupole splittings found for the neutral mercapto- and phosphido-bridged dimers compared to the large values determined for pentacoordinate iron complexes (e.g., Δ = 2.57 mm/sec for $Fe(CO)_5$) have been previously cited[36a] as evidence for the existence of hexacoordinate iron atoms in an $Fe_2(CO)_6X_2$ dimer, thereby indicating the presence of a stereochemically active metal–metal bond. Hence, the large increases in the observed quadrupole splittings[7a] in the $[Fe_2(CO)_6(P(CH_3)_2)_2]^n$ series from 0.65 mm/sec for $n = 0$ to 1.29 mm/sec for $n = 1-$ to 1.53 mm/sec for $n = 2-$ are compatible with the presumed large increase in the Fe–Fe distance in going from a two-electron to a "net" one-electron to a "net" no-electron Fe–Fe bond.

Although the orientation of the principal axes of the electric field gradient tensor is not known at each iron nucleus for these dimers, a rough calculation of Δ has been done[37] based on the assumption that the three principal axes for each iron atom lie approximately along the local coordinate system used for each iron atom. Although a linear correlation was not expected, the calculated values were found to increase similarly as the observed ones with the largest gradient lying in the x direction for the neutral species but along the z direction for the mono- and dianions presumably due to the "pile-up" of electron density in the bent Fe–Fe bond region.

Evidence which argues against the results reported here (viz., that the LUMO and the HOMO are highly metallic in character) is that in the Mössbauer spectrum of the $[Fe_2(CO)_6(P(CH_3)_2)_2]^-$ radical anion there is no indication of a magnetic hyperfine splitting into a six-line pattern expected for the interaction of the ^{57}Fe nuclei with the internal magnetic field of the unpaired electron. However, this may be due to the fact that the frequency of the electronic spin flipping is much larger than the Larmor frequency of the nuclear spin in the internal field as a result of a short spin–lattice relaxation time. Thus, the mean value of the internal field seen by the nuclei averages to zero, and hence in the absence of an applied external magnetic field no magnetic hyperfine structure is observed. This phenomenon is not uncommon for paramagnetic species.[38]

(e) Attractive P···P Interactions in the $[Fe_2(CO)_6(PR_2)_2]^n$ Series and Their Stereochemical Implications. The observation that interligand P···P contacts in phosphorus-bridged metal clusters can be as short as 2.54[39] and 2.57 Å[40] (which are only 0.3 Å greater than normal single-bond P–P distances) prompted us to examine the interligand P···P interactions in the $[Fe_2(CO)_6(PH_2)_2]^n$ series. To our initial surprise, the calculated overlap populations (Table X) are *positive* thereby indicating the existence of significant *attractive* P···P interactions, in contrast to the corresponding N···N interaction (Table X) in $Fe_2(CO)_6(NH_2)_2$ being slightly *repulsive*. As the interligand P···P distance is decreased from 2.86 Å (for $n = 0$) to 2.77 Å (for $n = 1-$) to 2.68 Å (for $n = 2-$), the attractive P···P interactions greatly increase to values commensurate with distinct bonding forces which, although still small relative to normal metal–ligand bonds, apparently produce pronounced geometrical deformations.[39,41] In each case, the $2a_2$(B)···$2a_2$(B′) interaction accounting for almost half of the total B···B overlap population involves the two in-plane electron-pair orbitals on the two trigonally hybridized B atoms (Figure 4). The much smaller N···N interaction found for the H_2N-bridged dimer is expected on the basis of the smaller orbital size of the more electronegative nitrogen atoms. The occurrence of significant interligand P···P residual bonding may be ascribed to the more diffuse phosphorus orbitals which interact to form a symmetric (bonding) a_1 and an antisymmetric (antibonding) b_1 combination. The antibonding combination, being of higher energy and hence closer to the metal 3d levels, donates more electron density to the metal orbital combinations of b_1 symmetry, thereby leading to a net attractive P···P bonding interaction. This is completely analogous to the interaction of the two essentially lone pairs in the bridging *cis*-$CH_3N{=}NCH_3$ ligand (i.e., the symmetric and antisymmetric combinations are slightly bonding and antibonding, respectively, between the two nitrogen atoms, and therefore a larger donation from the antisymmetric combination to the iron atoms should likewise lead to a slight strengthening of the N–N bond).

It is especially noteworthy that the changes in overlap between the phosphorus 3s orbitals parallel the changes in the

Table XI. Carbonyl Orbital Occupancies and Force Constants

Complex		5σ	$2\pi_x$	$2\pi_y$	k, mdyn/Å
$Fe_2(CO)_6(NCH_3)_2$	ax[a]	1.38	0.28	0.26	
	eq[b]	1.37	0.28	0.27	
$Fe_2(CO)_6(NH_2)_2$	ax	1.39	0.27	0.25	
	eq	1.37	0.24	0.29	
$Fe_2(CO)_6S_2$	ax	1.38	0.29	0.26	16.65[c]
	eq	1.37	0.27	0.29	16.39[c]
anti-$Fe_2(CO)_6(SCH_3)_2$	ax	1.38	0.28	0.27	16.54,[c] 16.13[d]
	eq	1.36	0.26	0.30	16.22,[c] 17.05[d]
syn-$Fe_2(CO)_6(SCH_3)_2$	ax	1.38	0.28	0.27	16.08,[d] 16.61[c]
	eq	1.36	0.26	0.30	17.01,[d] 16.16[c]
$Fe_2(CO)_6(PH_2)_2$[e]	ax	1.37	0.29	0.28	15.61,[d] 16.16[c]
	eq	1.35	0.27	0.30	16.53,[d] 15.89[c]
$[Fe_2(CO)_6(PH_2)_2]^-$[e]	ax	1.39	0.32	0.32	
	eq	1.36	0.31	0.35	
$[Fe_2(CO)_6(PH_2)_2]^{2-}$[e]	ax	1.39	0.36	0.37	13.21[d]
	eq	1.37	0.40	0.36	14.46[d]

[a] Axial. [b] Equatorial. [c] Reference 42d. [d] Reference 44. [e] Determined force constants are for the dimethylphosphido-bridged dimer.

$2a_1(P)\cdots 2a_1(P')$ overlap for the $[Fe_2(CO)_6(PH_2)_2]^n$ series with the increased overlap values from $n = 0$ to 2− expectedly associated with the decreased P···P distances. Hence, the dramatic increase in the attractive P···P interactions in $[Fe_2(CO)_6(PH_2)_2]^n$ upon reduction is consistent with ^1H NMR measurements[7a] showing a large increase in the magnitude of the $^{31}P\cdots^{31}P$ nuclear coupling constant $|J_{PP}|$ from 85 ± 10 ($n = 0$) to >500 Hz ($n = 2-$) for the dimethylphosphido-bridged iron carbonyl dimers, if direct orbital overlap between the bridging atoms is the predominant mechanism for the P···P nuclear coupling. However, we cannot rule out the possibility of spin polarization via Fe–P bonds which may be comparable to or even more important than the through-space coupling; further studies certainly need to be done to clarify this point.

Fe–C and C–O Bonding. Vibrational analyses of the infrared spectral data of various $Fe_2(CO)_6X_2$ molecules have been carried out by several groups,[25,42-44] and the results have been discussed in terms of qualitative bonding. Of particular relevance to our calculations is the extensive study by Dessy and Wieczorek[44] involving force constant calculations via the Cotton–Kraihanzel force field model for several neutral and reduced $[Fe_2(CO)_6X_2]^n$ systems (X = SCH_3 with $n = 0$, 1−; X = $P(CH_3)_2$ with $n = 0$, 2−; X = $As(CH_3)_2$ with $n = 0$, 2−). They determined that a one-step reduction of the syn or anti methylmercapto-bridged dimer from $n = 0$ to 1− decreased both the axial and equatorial C–O force constants, k^{ax} and k^{eq}, by ca. 1.0 mdyn/Å, and similarly the two-step reduction of the dimethylphosphido-bridged dimer from $n = 0$ to 2− decreased k^{ax} and k^{eq} by 2.4 and 2.1 mdyn/Å, respectively.

Our calculations suggest that the above results which show a weakening of the C–O bonds upon reduction can be attributed to a relative destabilization of the iron 3d orbitals upon reduction (Figure 5), which produces a smaller $5\sigma(CO) \rightarrow 3d(Fe)$ donation together with a larger $3d(Fe) \rightarrow 2\pi(CO)$ back-bonding and hence a strengthening of the Fe–C bonds and weakening of the C–O bonds. The calculated carbonyl orbital occupancies and some of the determined force constants are presented in Table XI. A comparison between the corresponding 5σ and 2π orbital occupancies for the mercapto-bridged and neutral phosphido-bridged dimers indicates no significant difference in the $5\sigma(CO) \rightarrow 3d(Fe)$ donation but significantly greater $3d(Fe) \rightarrow 2\pi(CO)$ back-bonding in the case of the neutral phosphido-bridged dimer thereby implying stronger Fe–C bonds and hence weaker C–O bonds. This correlation is in accord with the carbonyl force constants listed in Table XI.

A comparison of the axial Fe–C and C–O bonds with the equatorial ones (Table XI) indicates that (even though the differences are sufficiently small to be of borderline significance) the Fe–C(ax) bonds appear to be slightly weaker than the Fe–C(eq) ones based on the smaller $5\sigma(CO) \rightarrow 3d(Fe)$ donation and smaller $3d(Fe) \rightarrow 2\pi(CO)$ back-donation. Part of this small difference of possible significance may be attributed to the minute but significant antibonding character between the iron atom and its axial carbonyl in the HOMO of the neutral species. The C–O bond strength is harder to judge, since the σ and π effects act in the opposite direction. From the use of an empirical equation derived by Hall and Fenske[13] to correlate carbonyl orbital occupancies with force constants in octahedral-like metal carbonyl halides and dihalides, the axial and equatorial carbonyl force constants are calculated to be very similar. This is in accord with the sophisticated force constant calculations by Natile and Bor[42c,d] based upon isotopic frequencies for $Fe_2(CO)_6S_2$ (where $k^{ax} = 16.65 > k^{eq} = 16.39$ mdyn/Å) and for *anti*-$Fe_2(CO)_6(SCH_3)_2$ (where $k^{ax} = 16.54 > k^{eq} = 16.22$ mdyn/Å) but at variance with the large difference between k^{ax} and k^{eq} of ca. 1.0 mdyn/Å in the opposite direction obtained by Dessy and Wieczorek[44] from their simplified force field model.

Acknowledgment. We are most pleased to acknowledge financial support of this research by the National Science Foundation. B.K.T. is grateful for a University of Wisconsin predoctoral fellowship (Sept 1971–June 1972). We also are indebted to Dr. G. Bor for furnishing us with unpublished force constant data on several $Fe_2(CO)_6X_2$ molecules. The use of the UNIVAC 1108 computer at the Academic Computing Center, University of Wisconsin, Madison, Wis., was made available through partial support of the National Science Foundation and the Wisconsin Alumni Research Foundation administered through the University Research Committee.

Registry No. $Fe_2(CO)_6(NCH_3)_2$, 26814-32-4; $Fe_2(CO)_6(NH_2)_2$, 19705-87-4; $Fe_2(CO)_6S_2$, 14243-23-3; *anti*-$Fe_2(CO)_6(SCH_3)_2$, 19976-87-5; *syn*-$Fe_2(CO)_6(SCH_3)_2$, 19976-88-6; $Fe_2(CO)_6(PH_2)_2$, 56783-48-3; $[Fe_2(CO)_6(PH_2)_2]^-$, 56829-58-4; $[Fe_2(CO)_6(PH_2)_2]^{2-}$, 56783-49-4.

References and Notes

(1) Presented in part at the 165th National Meeting of the American Chemical Society, Dallas, Tex., April 1973; based in part upon a dissertation submitted by B. K. Teo to the Graduate School of the University of Wisconsin, Madison, Wis., in partial fulfillment of the requirements for the Ph.D. degree, 1973.
(2) Previous paper in this series: B. K. Teo, M. B. Hall, R. F. Fenske, and L. F. Dahl, *J. Organomet. Chem.*, **70**, 413 (1974).
(3) (a) L. F. Dahl, W. R. Costello, and R. B. King, *J. Am. Chem. Soc.*, **90**, 5422 (1968); (b) L. F. Dahl and C. H. Wei, *Inorg. Chem.*, **2**, 328 (1963); (c) W. Henslee and R. E. Davis, *Cryst. Struct. Commun.*, **1**, 403 (1972); (d) J. Huntsman and L. F. Dahl, to be submitted for publication; (e) P. M. Treichel, W. K. Dean, and J. C. Calabrese, *Inorg. Chem.*, **12**, 2908 (1973); (f) R. J. Doedens, *ibid.*, **7**, 2323 (1968); (g) J. A. J. Jarvis, B. E. Job, B. T. Kilbourn, R. H. B. Mais, P. G. Owston, and P. F. Todd, *Chem. Commun.*, 1149 (1967); J. Piron, P. Piret, and M. Van Meerssche, *Bull. Soc. Chim. Belg.*, **76**, 505 (1967); (h) B. K. Teo, M. F. Farona, and L. F. Dahl, to be submitted for publication; (i) P. E. Baikie and O. S. Mills, *Inorg. Chim. Acta*, **1**, 55 (1967); (j) H. P. Weber and R. F. Bryan, *J. Chem. Soc. A*, 182 (1967); (k) B. M. Gatehouse, *Chem. Commun.*, 948 (1969); A. S. Foust, Jr., Ph.D. Thesis, University of Wisconsin, Madison, Wis., 1970.
(4) (a) R. J. Doedens and J. A. Ibers, *Inorg. Chem.*, **8**, 2709 (1969); (b) R. J. Doedens, *ibid.*, **9**, 429 (1970); (c) R. G. Little and R. J. Doedens, *ibid.*, **11**, 1392 (1972); (d) C. H. Wei and L. F. Dahl, *ibid.*, **4**, 1 (1965); C. H. Wei and L. F. Dahl, *ibid.*, **4**, 493 (1965).
(5) A. J. Carty, D. P. Madden, M. Mathew, G. J. Palenik, and T. Birchall, *Chem. Commun.*, 1664 (1970).
(6) P. S. Braterman, *Struct. Bonding (Berlin)*, **10**, 57 (1971).
(7) (a) R. E. Dessy, A. L. Rheingold, and G. D. Howard, *J. Am. Chem. Soc.*, **94**, 746 (1972); (b) R. E. Dessy and L. A. Bares, *Acc. Chem. Res.*, **5**, 415 (1972).

(8) J. M. Coleman and L. F. Dahl, *J. Am. Chem. Soc.*, **89**, 542 (1967).
(9) (a) M. B. Hall and R. F. Fenske, *Inorg. Chem.*, **11**, 768 (1972); (b) M. B. Hall, Ph.D. Thesis, University of Wisconsin, Madison, Wis., 1971; (c) R. F. Fenske, *Pure Appl. Chem.*, **27**, 61 (1971).
(10) E. Clementi, *J. Chem. Phys.*, **40**, 1944 (1964).
(11) W. J. Hehre, R. F. Stewart, and J. A. Pople, *J. Chem. Phys.*, **51**, 2657 (1969).
(12) J. W. Richardson, W. C. Nieuwpoort, R. R. Powell, and W. F. Edgell, *J. Chem. Phys.*, **36**, 1057 (1962).
(13) M. B. Hall and R. F. Fenske, *Inorg. Chem.*, **11**, 1619 (1972).
(14) (a) R. L. DeKock, A. C. Sarapu, and R. F. Fenske, *Inorg. Chem.*, **10**, 38 (1971); (b) R. F. Fenske and R. L. DeKock, *ibid.*, **11**, 437 (1972); (c) A. C. Sarapu and R. F. Fenske, *ibid.*, **11**, 3021 (1972); (d) D. L. Lichtenberger, A. C. Sarapu, and R. F. Fenske, *ibid.*, **12**, 702 (1973); (e) D. L. Lichtenberger and R. F. Fenske, *ibid.*, **13**, 486 (1974); (f) A. C. Sarapu and R. F. Fenske, *ibid.*, **14**, 247 (1975); (g) J. L. Petersen, D. L. Lichtenberger, R. F. Fenske, and L. F. Dahl, *J. Am. Chem. Soc.*, **97**, 6433 (1975).
(15) (a) N. G. Connelly and L. F. Dahl, *J. Am. Chem. Soc.*, **92**, 7472 (1970); (b) J. D. Sinclair, N. G. Connelly, and L. F. Dahl, to be submitted for publication.
(16) *Chem. Soc., Spec. Publ.*, **No. 18**, S7s, S9s (1965).
(17) The computed populations and gross atomic charges [R. S. Mulliken, *J. Chem. Phys.*, **23**, 1833, 1844, 2338, 2343 (1955)] utilized in this paper are as follows: (a) the overlap population between two atoms k and l in a given molecular orbital $\psi_i = \sum_{r_k} \chi_{r_k} C_{r_k i}$ is given by $OP(i;k,l) = \sum_{r_k}\sum_{s_l} 2N(i) C_{r_k i} C_{s_l i} S(r_k,s_l)$, where C_{r_k} and C_{s_l} are coefficients of the *valence* orbitals χ_{r_k} and χ_{s_l} on atoms k and l, respectively, in the ith molecular orbital populated with $N(i)$ electrons and where $S(r_k,s_l)$ represents the overlap between χ_{r_k} and χ_{s_l}; (b) the total overlap population between atoms k and l is given by $OP(k,l) = \sum_i \sum_{r_k} \sum_{s_l} 2N(i) C_{r_k} C_{s_l} S(r_k,s_l)$, where the first summation is over all occupied molecular orbitals; (c) the calculated gross atomic charge, q_k, on atom k is then $q_k = Z_k - \sum_{r_k} n(r_k)$ where Z_k denotes the bare nuclear charge for center k and the second term represents the total population obtained by a summation over all valence and core atomic orbitals on center k; $n(r_k) = \sum_i n(i,r_k)$ where $n(i;r_k) = N(i) C_{r_k i} [C_{r_k i} + \sum_{l \neq k} C_{s_l i} S(r_k,s_l)]$.
(18) D. A. Brown, *J. Chem. Phys.*, **33**, 1037 (1960).
(19) In spite of their similarity based upon qualitative electron orbital bookkeeping, the bonding characteristics of the $Fe_2(CO)_6X_2$ dimers are markedly different from those of the carbonyl-bridged $Co_2(CO)_8$ isomer. A comparison of the eigenvectors and eigenvalues obtained from a molecular orbital calculation[20] of $Co_2(CO)_8$ with those presented here for representative $Fe_2(CO)_6X_2$ molecules reveals in contradistinction to the iron dimers that the carbonyl-bridged $Co_2(CO)_2$ orbital interactions are best considered as delocalized multicentered bonds such that no reasonable separation between the metal–metal and metal–ligand bonds is feasible. The suggestion of nonseparable multicentered linkages of bridging carbonyl ligands to two or three metals has been put forth from qualitative considerations by P. Chini *Inorg. Chim. Acta, Rev.*, **2**, 31 (1968), and by Braterman.[6]
(20) B. K. Teo, M. B. Hall, R. F. Fenske, and L. F. Dahl, to be submitted for publication.
(21) In contrast, SCCC calculations[22] of $Mn_2(CO)_{10}$ and Fenske–Hall-type MO calculations[20] of $Mn_2(CO)_{10}$ and the $[Cr_2(CO)_{10}]^{2-}$ dianion indicated that a highly significant cross interaction occurs between the σ-like orbitals of one metal (e.g., comprised of 18% $3d_{z^2}$, 2% 4s, and 13% p_z character in $Mn_2(CO)_{10}$)[20] and the π^* orbitals of the equatorial carbonyl ligands coordinated to the other metal and that this cross interaction contributes about half of the HOMO–LUMO splitting. Hence, in a sense the bent Fe–Fe bonds in the ligand-bridged $Fe_2(CO)_6X_2$ complexes may be considered as "purer" than the metal–metal bonds in the $Mn_2(CO)_{10}$-type dimers.
(22) D. A. Brown, W. J. Chambers, N. J. Fitzpatrick, and R. M. Rawlinson, *J. Chem. Soc. A*, 720 (1971).
(23) The electron density maps were calculated and plotted via a local program "MOPLOT": D. L. Lichtenberger, Ph.D. Thesis (Appendix), University of Wisconsin, Madison, Wis., 1974.
(24) (a) E. Kochanski and J. M. Lehn, *Theor. Chim. Acta*, **14**, 281 (1969); (b) M. D. Newton and J. M. Schulman, *J. Am. Chem. Soc.*, **94**, 767 (1972).
(25) W. M. Scovell and T. G. Spiro, *Inorg. Chem.*, **13**, 304 (1974).
(26) E. Bayer, H. Eckstein, H. Hagenmaier, D. Josef, J. Koch, P. Krauss, A. Roder, and P. Schretzmann, *Eur. J. Biochem.*, **8**, 33 (1969).
(27) The most striking feature is the large separation of 4.8 eV between the stabilized $5a_1$ and destabilized $4b_1$ orbitals associated with the σ-like "lone pairs".[28] A large part of the σ donation comes from the $4b_1$ orbital (which is closer in energy to the 3d metal orbitals) rather than from the $5a_1$ orbital.
(28) Although no direct measurement of this splitting has yet been made, a value of 3.3 (2) eV was suggested for the corresponding splitting in *trans*-$CH_3N{=}NCH_3$ from gas-phase photoelectron spectroscopy: E. Haselbach, J. A. Hashmall, E. Heilbronner, and V. Hornung, *Angew. Chem., Int. Ed. Engl.*, **8**, 878 (1969); E. Haselbach and E. Heilbronner, *Helv. Chim. Acta*, **53**, 684 (1970); K. N. Houk, Y. M. Chang, and P. S. Engel, *J. Am. Chem. Soc.*, **97**, 1824 (1975).
(29) L. Pauling, "The Nature of the Chemical Bond", 3rd ed, Cornell University Press, Ithaca, N.Y., 1971, p 228.
(30) F. A. Cotton and G. Wilkinson, "Advanced Inorganic Chemistry", 3rd ed, Interscience, New York, N.Y., 1972, p 117. It should also be noted that the S–S stretching constant was found by Scovell and Spiro[25] to be 2.50 mdyn/Å, in agreement with the same value given by Wilson et al.[31] for S_2H_2.
(31) E. B. Wilson, Jr., J. D. Decius, and P. C. Cross, "Molecular Vibrations", McGraw-Hill, New York, N.Y., 1955.
(32) C. H. Wei, L. Markó, G. Bor, and L. F. Dahl, *J. Am. Chem. Soc.*, **95**, 4840 (1973).
(33) B. K. Teo and L. F. Dahl, to be submitted for publication.
(34) The large charge difference between P and S (calculated with no inclusion of the virtual 3d AO's) has a crucial implication of Fe–X bonding. That is, as the positive atomic charge on P increases, the virtual, highly diffused 3d phosphorus orbital(s) will be more stabilized and will become closer to the metal 3d orbitals such that back-donation from the filled metal orbital combinations into the phosphorus 3d orbital(s) will be enhanced, thereby reducing to some extent the high positive charge on the phosphorus atoms. A magnified $d\pi(M) \rightarrow d\pi(P)$ bonding for PR_2- relative to analogous SR-bridged complexes is consistent with the shorter observed M–P(bridging) bond lengths compared to corresponding M–S(bridging) bond lengths: cf. L. F. Dahl, J. D. Sinclair, and B. K. Teo in "The Organic Chemistry of Iron", E. A. Koerner von Gustorf, Ed., Academic Press, New York, N.Y.
(35) For an excellent discussion of the time scales for the principal structural techniques capable of detecting variant electronic state lifetimes, see E. L. Muetterties, *Inorg. Chem.*, **4**, 769 (1965); R. H. Holm, B. A. Averill, T. Herskovitz, R. B. Frankel, H. B. Gray, O. Siiman, and F. J. Grunthaner, *J. Am. Chem. Soc.*, **96**, 2644 (1974).
(36) (a) T. C. Gibb, R. Greatrex, N. N. Greenwood, and D. T. Thompson, *J. Chem. Soc., A*, 1663 (1967); (b) R. Greatrex and N. N. Greenwood, *Discuss. Faraday Soc.*, **No. 47**, 126 (1969); (c) E. Šimánek and Z. Šroubek, *Phys. Rev.*, **163**, 275 (1967).
(37) B. K. Teo, Ph.D. Thesis, University of Wisonsin, Madison, Wis., 1973.
(38) (a) J. Danon in "Physical Methods in Advanced Inorganic Chemistry", H. A. O. Hill and P. Day, Ed., Interscience, New York, N.Y., 1968, p 404; (b) J. R. Sams and T. B. Tsin, *Inorg. Chem.*, **14**, 1573 (1975).
(39) R. C. Ryan and L. F. Dahl, *J. Am. Chem. Soc.*, in press.
(40) G. L. Simon and L. F. Dahl, *J. Am. Chem. Soc.*, **95**, 2175 (1973).
(41) Inclusion in the calculations of virtual 3d AO's on each phosphorus atom would be expected to increase the total P···P overlap populations, indicative of even greater attractive residual forces in the $[Fe_2(CO)_6(PH_2)_2]^n$ series.
(42) (a) G. Bor, *J. Organomet. Chem.*, **11**, 195 (1968); (b) G. Bor, *Discuss. Faraday Soc.*, **No. 47**, 64, 65, 68 (1969); (c) G. Natile and G. Bor, private communication to L. F. Dahl and B. K. Teo, 1973; (d) G. Bor, *J. Organomet. Chem.*, **94**, 181 (1975).
(43) M. L. N. Reddy and D. S. Urch, *Discuss. Faraday Soc.*, **No. 47**, 53, 66, 68 (1969).
(44) R. E. Dessy and L. Wieczorek, *J. Am. Chem. Soc.*, **91**, 4963 (1969).